

# Application of Bruggeman and Maxwell Garnett homogenization formalisms to random composite materials containing dimers

Tom G. Mackay\*

*School of Mathematics and Maxwell Institute for Mathematical Sciences  
University of Edinburgh, Edinburgh EH9 3FD, UK*

and

*NanoMM — Nanoengineered Metamaterials Group  
Department of Engineering Science and Mechanics  
Pennsylvania State University, University Park, PA 16802-6812, USA*

Akhlesh Lakhtakia†

*NanoMM — Nanoengineered Metamaterials Group  
Department of Engineering Science and Mechanics  
Pennsylvania State University, University Park, PA 16802-6812, USA*

## Abstract

The homogenization of a composite material comprising three isotropic dielectric materials was investigated. The component materials were randomly distributed as spherical particles, with the particles of two of the component materials being coupled to form dimers. The Bruggeman and Maxwell Garnett formalisms were developed to estimate the permittivity dyadic of the homogenized composite material (HCM), under the quasi-electrostatic approximation. Both randomly oriented and identically oriented dimers were accommodated; in the former case the HCM is isotropic, whereas in the latter case the HCM is uniaxial. Representative numerical results for composite materials containing dielectric–dielectric dimers demonstrate close agreement between the estimates delivered by the Bruggeman and Maxwell Garnett formalisms. For composite materials containing metal–dielectric dimers with moderate degrees of dissipation, the estimates of the two formalisms are in broad agreement, provided that the dimer volume fractions are relatively low. In general, the effects of intradimer coupling on the estimates of the HCM permittivity are relatively modest but not insignificant, these effects being exacerbated by anisotropy when all dimers are identically oriented.

**Keywords:** depolarization; homogenization; Bruggeman formalism; Maxwell Garnett formalism; dimer; quasi-electrostatic approximation; polarizability density

## 1 Introduction

Composite materials containing random dispersals of particles or inclusions can exhibit remarkable characteristics if two (or more) of their component materials are coupled together to form dimers (or trimers,

---

\*E-mail: T.Mackay@ed.ac.uk.

†E-mail: akhlesh@psu.edu

etc.). Indeed, nanoengineered composite materials containing dimeric particles are playing an increasingly prominent role in the development of new technologies [1]. For example, plasmonic interactions in metallic dimers can result in enhanced Raman scattering or molecular fluorescence [2, 3, 4], which may lead to highly sensitive optical sensors. Dielectric dimers are also of considerable interest, in the context of Mott insulators [5, 6], liquid crystals [7], and interstellar molecular hydrogen formation [8], for examples.

This study concerns the estimation of the effective constitutive parameters of particulate composite materials, wherein two of the component materials are jointly present as dimers. Previously this topic has been investigated using Mie scattering theory [9], a Brownian-motion formulation [10], numerical methods such as the finite element method [2], and quantum-mechanical methods based on density function theory [4, 8]. In contrast, the theoretical approaches taken herein are simpler, being based on the well-established homogenization formalisms named after Bruggeman and Maxwell Garnett [11, 12]. The Bruggeman formalism is a self-consistent one in which all component materials are treated in an identical manner. A rigorous basis for the Bruggeman formalism arises from the strong-permittivity-fluctuation theory [13]. The nature of the Maxwell Garnett formalism is essentially perturbative—which is only appropriate for dilute dispersals of particles in a host material [14, 15]. The theoretical basis for the Maxwell Garnett formalism is bolstered by its close association with the Hashin–Shtrikman bounds [16].

The plan of this paper is as follows. Relevant details of the homogenization formalisms are provided in §2. This is followed by the development of appropriate expressions for the electric dipole moments and polarizability densities in §3. The homogenization formalisms themselves are set up for composite materials containing identically oriented dimers in §4 and randomly oriented dimers in §5. Representative numerical results are presented in §6 for both dielectric–dielectric dimers and metal–dielectric dimers. Lastly, a brief discussion of the theory and numerical results is provided in §7. As regards notation: the permittivity of free space is written as  $\varepsilon_0$ ;  $c_0$  denotes the speed of light in free space;  $\omega$  is the angular frequency; and  $i = \sqrt{-1}$ . Vectors are underlined (with the  $\hat{\phantom{a}}$  symbol denoting unit vectors), whereas dyadics [17, 18] are double underlined.

## 2 Homogenization preliminaries

The homogenization of three isotropic component materials, labeled as ‘a’, ‘b’, and ‘c’, of a particulate composite material is investigated in the following sections. The three component materials are characterized by the permittivity scalars  $\varepsilon_a$ ,  $\varepsilon_b$ , and  $\varepsilon_c$ .

Component materials ‘a’ and ‘b’ are dispersed as dimers of electrically small spheres. For simplicity, the average radiuses of the spheres belonging to these two component materials are taken to be the same, namely  $s$ . Each sphere of component material ‘a’ is chemically linked to exactly one sphere of component material ‘b’, thus forming a dimer. The distance between the centers of the two spheres making up a dimer is  $d \geq 2s$ . In each dimer, the location of the center of the ‘b’ sphere relative to the center of the ‘a’ sphere is given by  $d\hat{\underline{d}}$ , where the unit vector

$$\hat{\underline{d}} = (\hat{\underline{u}}_x \cos \phi + \hat{\underline{u}}_y \sin \phi) \sin \theta + \hat{\underline{u}}_z \cos \theta, \quad \theta \in [0, \pi], \quad \phi \in [0, 2\pi]. \quad (1)$$

A heterodimer is specified by  $\varepsilon_a \neq \varepsilon_b$ , whereas a homodimer is specified by  $\varepsilon_a = \varepsilon_b$ . The dimers are randomly distributed.

When applying the Bruggeman formalism, component material ‘c’ is regarded as a random dispersal of electrically small spheres, which we take to have an average radius  $s$ . No particular topology is assigned to component material ‘c’ in the Maxwell Garnett formalism. The volume fractions of component materials ‘a’, ‘b’, and ‘c’ are  $f_a$ ,  $f_b$ , and  $f_c$ , respectively, with  $f_a = f_b$  and  $f_a + f_b + f_c = 1$ .

Provided that the largest relevant wavelength is much longer than the linear dimensions of the spheres and the dimers, the mixture of component materials ‘a’, ‘b’, and ‘c’ may be regarded as being effectively homogeneous. The constitutive parameters of the resulting homogenized composite material (HCM) may be estimated using a homogenization formalism. Two distinct cases are investigated theoretically: identically oriented dimers are the subject of §4, while randomly oriented dimers are treated in §5.

All dimers are assumed to be oriented in the same direction in §4; i.e.,  $\hat{\underline{d}}$  is fixed for all dimers. Consequently, the HCM is a uniaxial dielectric material characterized by a permittivity dyadic of the form

$$\underline{\underline{\varepsilon}}_{HCM} = \varepsilon_{HCM}^{\perp} \left( \underline{\underline{I}} - \hat{\underline{d}}\hat{\underline{d}} \right) + \varepsilon_{HCM}^{\parallel} \hat{\underline{d}}\hat{\underline{d}}, \quad (2)$$

where  $\underline{\underline{I}}$  is the identity dyadic. The estimate of  $\underline{\underline{\varepsilon}}_{HCM}$  (with components  $\varepsilon_{HCM}^{\perp}$  and  $\varepsilon_{HCM}^{\parallel}$ ) yielded by the Bruggeman formalism is written as  $\underline{\underline{\varepsilon}}_{Br}$  (with components  $\varepsilon_{Br}^{\perp}$  and  $\varepsilon_{Br}^{\parallel}$ ) and the estimate yielded by the Maxwell Garnett formalism is written as  $\underline{\underline{\varepsilon}}_{MG}$  (with components  $\varepsilon_{MG}^{\perp}$  and  $\varepsilon_{MG}^{\parallel}$ ).

As the dimers are taken to have no preferred orientation in §5, the corresponding HCM is an isotropic dielectric material characterized by the scalar permittivity  $\varepsilon_{HCM}$ . The estimate of  $\varepsilon_{HCM}$  yielded by the Bruggeman formalism is written as  $\varepsilon_{Br}$ , and the estimate yielded by the Maxwell Garnett formalism is written as  $\varepsilon_{MG}$ .

### 3 Electric dipole moments and polarizability densities

A quasi-electrostatic viewpoint is adopted in both homogenization formalisms, whereby each pair of electrically small spheres comprising a dimer is modeled as a pair of electric dipole moments  $\underline{p}_a$  and  $\underline{p}_b$ , separated by the distance  $d$  in the direction of  $\hat{\underline{d}}$ . In the case of the Bruggeman formalism, each electrically small sphere of component ‘c’ is modeled as a electric dipole moment  $\underline{p}_c$ . No magnetic dipole moments analogous to  $\underline{p}_{a,b,c}$  are present in the quasi-electrostatic regime.

We need to consider two separate cases. In §3.1 the electrically small spheres are immersed in a homogeneous uniaxial dielectric material, while in §3.2 the electrically small spheres are immersed in a homogeneous isotropic dielectric material.

#### 3.1 Uniaxial dielectric immersion material

Let us consider a single dimer immersed in a homogeneous dielectric material characterized by the permittivity dyadic  $\underline{\underline{\varepsilon}}_{out}$ . In this section,  $\underline{\underline{\varepsilon}}_{out}$  characterizes a uniaxial material whose distinguished axis is parallel to  $\hat{\underline{d}}$ ; i.e.,

$$\underline{\underline{\varepsilon}}_{out} = \varepsilon_{out}^{\perp} \left( \underline{\underline{I}} - \hat{\underline{d}}\hat{\underline{d}} \right) + \varepsilon_{out}^{\parallel} \hat{\underline{d}}\hat{\underline{d}}. \quad (3)$$

The dimer is taken to be centered at the origin  $\underline{r} = \underline{0}$ .

A quasi-electrostatic field, originating from a distant source, is incident on this dimer. The incident electric field phasor is denoted by  $\underline{E}_{inc}(\underline{r})$ . In response to  $\underline{E}_{inc}(\underline{r})$ , electric dipole moments  $\underline{p}_a$  and  $\underline{p}_b$  are induced at  $\underline{r}_a = -(d/2)\hat{\underline{d}}$  and  $\underline{r}_b = (d/2)\hat{\underline{d}}$ , respectively. These electric dipole moments are given by [19]

$$\underline{p}_{\ell} = \frac{4}{3}\pi s^3 \underline{\underline{\alpha}}_{\ell/out} \cdot \underline{E}_{exc}(\underline{r}_{\ell}), \quad \ell \in \{a, b\}, \quad (4)$$

where

$$\underline{\underline{\alpha}}_{\ell/out} = \left( \varepsilon_{\ell} \underline{\underline{I}} - \underline{\underline{\varepsilon}}_{out} \right) \cdot \left[ \underline{\underline{I}} + i\omega \underline{\underline{D}}_{out} \cdot \left( \varepsilon_{\ell} \underline{\underline{I}} - \underline{\underline{\varepsilon}}_{out} \right) \right]^{-1} \quad (5)$$

is the polarizability density dyadic of an isolated sphere of material ‘ $\ell$ ’, immersed in the material labeled ‘out’, with  $\underline{\underline{D}}_{out}$  being the corresponding depolarization dyadic [18].

The  $3 \times 3$  dyadics  $\underline{\underline{D}}_{out}$  and  $\underline{\underline{\alpha}}_{\ell/out}$  possess the same symmetric form as  $\underline{\underline{\varepsilon}}_{out}$ , i.e.,

$$\left. \begin{aligned} \underline{\underline{D}}_{out} &= D_{out}^{\perp} \left( \underline{\underline{I}} - \hat{\underline{d}}\hat{\underline{d}} \right) + D_{out}^{\parallel} \hat{\underline{d}}\hat{\underline{d}} \\ \underline{\underline{\alpha}}_{\ell/out} &= \alpha_{\ell/out}^{\perp} \left( \underline{\underline{I}} - \hat{\underline{d}}\hat{\underline{d}} \right) + \alpha_{\ell/out}^{\parallel} \hat{\underline{d}}\hat{\underline{d}} \end{aligned} \right\}. \quad (6)$$

The components of  $\underline{\underline{D}}_{out}$  are given as [20]

$$\left. \begin{aligned} D_{out}^\perp &= \frac{\gamma}{i\omega\varepsilon_{out}^\perp} L^\perp(\gamma) \\ D_{out}^\parallel &= \frac{1}{i\omega\varepsilon_{out}^\perp} L^\parallel(\gamma) \end{aligned} \right\}, \quad (7)$$

with

$$\left. \begin{aligned} L^\perp(\gamma) &= \frac{1}{2\gamma} \left[ \frac{1}{\sqrt{1-\gamma}} \tanh^{-1}(\sqrt{1-\gamma}) - L^\parallel(\gamma) \right] \\ L^\parallel(\gamma) &= \frac{1}{\gamma-1} \left[ 1 - \frac{1}{\sqrt{1-\gamma}} \tanh^{-1}(\sqrt{1-\gamma}) \right] \end{aligned} \right\} \quad (8)$$

being dimensionless scalar functions of the dimensionless parameter  $\gamma = \varepsilon_{out}^\parallel / \varepsilon_{out}^\perp$ . The components of  $\underline{\underline{\alpha}}_{\ell/out}$  are given as

$$\left. \begin{aligned} \alpha_{\ell/out}^\perp &= \frac{\varepsilon_{out}^\perp (\varepsilon_\ell - \varepsilon_{out}^\perp)}{\varepsilon_{out}^\perp + \gamma L^\perp(\gamma) (\varepsilon_\ell - \varepsilon_{out}^\perp)} \\ \alpha_{\ell/out}^\parallel &= \frac{\varepsilon_{out}^\perp (\varepsilon_\ell - \varepsilon_{out}^\parallel)}{\varepsilon_{out}^\perp + L^\parallel(\gamma) (\varepsilon_\ell - \varepsilon_{out}^\parallel)} \end{aligned} \right\}. \quad (9)$$

The electric field phasor  $\underline{E}_{exc}(\underline{r}_a)$  exciting the sphere of material ‘a’ is not merely  $\underline{E}_{inc}(\underline{r}_a)$ ; instead,

$$\underline{E}_{exc}(\underline{r}_a) = \underline{E}_{inc}(\underline{r}_a) + \underline{E}_{sca}^b(\underline{r}_a), \quad (10)$$

where  $\underline{E}_{sca}^b$  represents the electric field scattered by the sphere of material ‘b’. Likewise, there are two contributions to  $\underline{E}_{exc}(\underline{r}_b)$ ; i.e.,

$$\underline{E}_{exc}(\underline{r}_b) = \underline{E}_{inc}(\underline{r}_b) + \underline{E}_{sca}^a(\underline{r}_b), \quad (11)$$

where  $\underline{E}_{sca}^a$  represents the electric field scattered by the sphere of material ‘a’. In the quasi-electrostatic regime,  $\underline{E}_{inc}(\underline{r}_a) \simeq \underline{E}_{inc}(\underline{r}_b) \simeq \underline{E}_{inc}(\mathbf{0})$  and the scattered field phasors are given by [17, Sec. 10.5]

$$\left. \begin{aligned} \underline{E}_{sca}^a(\underline{r}_b) &= \frac{1}{4\pi\varepsilon_{out}^\perp d^3} \left[ 2\hat{\underline{d}}\hat{\underline{d}} - \gamma \left( \underline{\underline{I}} - \hat{\underline{d}}\hat{\underline{d}} \right) \right] \cdot \underline{p}_a \\ \underline{E}_{sca}^b(\underline{r}_a) &= \frac{1}{4\pi\varepsilon_{out}^\perp d^3} \left[ 2\hat{\underline{d}}\hat{\underline{d}} - \gamma \left( \underline{\underline{I}} - \hat{\underline{d}}\hat{\underline{d}} \right) \right] \cdot \underline{p}_b \end{aligned} \right\}. \quad (12)$$

The combination of Eqs. (4), (10), (11), and (12) yields

$$\left. \begin{aligned} \underline{p}_a - \sigma_\perp \underline{\underline{\alpha}}_{a/out} \cdot \left[ 2\hat{\underline{d}}\hat{\underline{d}} - \gamma \left( \underline{\underline{I}} - \hat{\underline{d}}\hat{\underline{d}} \right) \right] \cdot \underline{p}_b &= \frac{4}{3}\pi s^3 \underline{\underline{\alpha}}_{a/out} \cdot \underline{E}_{inc}(\mathbf{0}) \\ \underline{p}_b - \sigma_\perp \underline{\underline{\alpha}}_{b/out} \cdot \left[ 2\hat{\underline{d}}\hat{\underline{d}} - \gamma \left( \underline{\underline{I}} - \hat{\underline{d}}\hat{\underline{d}} \right) \right] \cdot \underline{p}_a &= \frac{4}{3}\pi s^3 \underline{\underline{\alpha}}_{b/out} \cdot \underline{E}_{inc}(\mathbf{0}) \end{aligned} \right\}, \quad (13)$$

wherein the parameter

$$\sigma_\perp = \frac{s^3}{3\varepsilon_{out}^\perp d^3}. \quad (14)$$

The pair of linear Eqs. (13) deliver the electric dipole moment

$$\underline{p}_\ell = \frac{4}{3}\pi s^3 \underline{\underline{\tilde{\alpha}}}_{\ell/out} \cdot \underline{E}_{inc}(\mathbf{0}), \quad \ell \in \{a, b\}, \quad (15)$$

with the  $3 \times 3$  dyadic function

$$\begin{aligned} \underline{\tilde{\alpha}}_{\ell/out} = & \left[ \left( 1 - \sigma_{\perp}^2 \gamma^2 \alpha_{a/out}^{\perp} \alpha_{b/out}^{\perp} \right) \left( \underline{\underline{I}} - \hat{\underline{d}} \hat{\underline{d}} \right) + \left( 1 - 4\sigma_{\perp}^2 \alpha_{a/out}^{\parallel} \alpha_{b/out}^{\parallel} \right) \hat{\underline{d}} \hat{\underline{d}} \right]^{-1} \\ & \cdot \left[ \left( \alpha_{\ell/out}^{\perp} - \sigma_{\perp} \gamma \alpha_{a/out}^{\perp} \alpha_{b/out}^{\perp} \right) \left( \underline{\underline{I}} - \hat{\underline{d}} \hat{\underline{d}} \right) + \left( \alpha_{\ell/out}^{\parallel} + 2\sigma_{\perp} \alpha_{a/out}^{\parallel} \alpha_{b/out}^{\parallel} \right) \hat{\underline{d}} \hat{\underline{d}} \right]. \end{aligned} \quad (16)$$

The dyadic  $\underline{\tilde{\alpha}}_{\ell/out} \neq \underline{\alpha}_{\ell/out}$  is the polarizability density dyadic of a monomer (sphere) of material ‘ $\ell$ ’ as a constituent of an isolated dimer immersed in the material labeled ‘out’. The sum

$$\underline{\alpha}_{dimer/out} = \underline{\tilde{\alpha}}_{a/out} + \underline{\tilde{\alpha}}_{b/out} \quad (17)$$

may be regarded as the polarizability density dyadic of the dimer, and the electric dipole moment

$$\underline{p}_{dimer} = \underline{p}_a + \underline{p}_b = \frac{4}{3} \pi s^3 \underline{\alpha}_{dimer/out} \cdot \underline{E}_{inc}(\underline{0}) \quad (18)$$

characterizes the quasi-static scattering response of the dimer. Although a uniaxial object [21], the dimer is different from a rod or a needle because the volume entering the right side of Eq. (18) is that of a sphere but not of a cylinder.

Next, let us turn to the electrically small sphere of material ‘ $c$ ’ immersed in a uniaxial dielectric material characterized by the permittivity dyadic  $\underline{\underline{\varepsilon}}_{out}$  given in Eq. (3). The sphere is centered at the origin  $\underline{r} = \underline{0}$ . Suppose that the sphere is illuminated by a quasi-electrostatic field  $\underline{E}_{inc}(\underline{r})$ . The induced electric dipole moment is given by [19]

$$\underline{p}_c = \frac{4}{3} \pi s^3 \underline{\alpha}_{c/out} \cdot \underline{E}_{inc}(\underline{0}), \quad (19)$$

where the polarizability density dyadic  $\underline{\alpha}_{c/out}$  is defined per Eq. (5) but with  $\varepsilon_{\ell}$  therein replaced by  $\varepsilon_c$ , and the components of  $\underline{\alpha}_{c/out}$  are written as  $\alpha_{c/out}^{\perp}$  and  $\alpha_{c/out}^{\parallel}$  per Eq. (6)<sub>2</sub>.

### 3.2 Isotropic dielectric immersion material

Suppose that the immersion material is isotropic, i.e.,  $\underline{\underline{\varepsilon}}_{out} = \varepsilon_{out} \underline{\underline{I}}$ . Then, the derivations in §3.1 simply considerably. In particular, the depolarization dyadic  $\underline{D}_{out}$  reduces to  $(3i\omega\varepsilon_{out})^{-1} \underline{\underline{I}}$ , while the polarizability density dyadic  $\underline{\alpha}_{\ell/out}$  reduces to  $\alpha_{\ell/out} \underline{\underline{I}}$ , where the polarizability density scalar

$$\alpha_{\ell/out} = 3\varepsilon_{out} \left( \frac{\varepsilon_{\ell} - \varepsilon_{out}}{\varepsilon_{\ell} + 2\varepsilon_{out}} \right), \quad \ell \in \{a, b\}. \quad (20)$$

Consequently, we get

$$\left. \begin{aligned} \underline{\tilde{\alpha}}_{a/out} &= \left[ \left( 1 - \sigma^2 \alpha_{a/out} \alpha_{b/out} \right) \left( \underline{\underline{I}} - \hat{\underline{d}} \hat{\underline{d}} \right) + \left( 1 - 4\sigma^2 \alpha_{a/out} \alpha_{b/out} \right) \hat{\underline{d}} \hat{\underline{d}} \right]^{-1} \\ &\quad \cdot \left[ \left( 1 - \sigma \alpha_{b/out} \right) \left( \underline{\underline{I}} - \hat{\underline{d}} \hat{\underline{d}} \right) + \left( 1 + 2\sigma \alpha_{b/out} \right) \hat{\underline{d}} \hat{\underline{d}} \right] \alpha_{a/out} \\ \underline{\tilde{\alpha}}_{b/out} &= \left[ \left( 1 - \sigma^2 \alpha_{a/out} \alpha_{b/out} \right) \left( \underline{\underline{I}} - \hat{\underline{d}} \hat{\underline{d}} \right) + \left( 1 - 4\sigma^2 \alpha_{a/out} \alpha_{b/out} \right) \hat{\underline{d}} \hat{\underline{d}} \right]^{-1} \\ &\quad \cdot \left[ \left( 1 - \sigma \alpha_{a/out} \right) \left( \underline{\underline{I}} - \hat{\underline{d}} \hat{\underline{d}} \right) + \left( 1 + 2\sigma \alpha_{a/out} \right) \hat{\underline{d}} \hat{\underline{d}} \right] \alpha_{b/out} \end{aligned} \right\}, \quad (21)$$

wherein the parameter

$$\sigma = \frac{s^3}{3\varepsilon_{out} d^3}. \quad (22)$$

These simple expressions are useful when the homogenization of a composite material containing randomly oriented dimers is considered.

The special case of homodimers is noteworthy. Here  $\varepsilon_a = \varepsilon_b$  and thus  $\alpha_{a/out} = \alpha_{b/out}$ . Hence,  $\underline{\tilde{\alpha}}_{a/out} = \underline{\tilde{\alpha}}_{b/out}$  with

$$\underline{\tilde{\alpha}}_{a/out}(\tilde{\sigma}) = \left[ (1 - \tilde{\sigma}^2) \left( \underline{\underline{I}} - \hat{\underline{d}}\hat{\underline{d}} \right) + (1 - 4\tilde{\sigma}^2) \hat{\underline{d}}\hat{\underline{d}} \right]^{-1} \cdot \left[ (1 - \tilde{\sigma}) \left( \underline{\underline{I}} - \hat{\underline{d}}\hat{\underline{d}} \right) + (1 + 2\tilde{\sigma}) \hat{\underline{d}}\hat{\underline{d}} \right] \alpha_{a/out}, \quad (23)$$

and the dimensionless scalar parameter

$$\tilde{\sigma} = \left( \frac{\varepsilon_a - \varepsilon_{out}}{\varepsilon_a + 2\varepsilon_{out}} \right) \frac{s^3}{d^3}. \quad (24)$$

The electric dipole moment of an electrically small sphere of material ‘c’ is given as in Eq. (19) with  $\underline{\alpha}_{c/out} = \alpha_{c/out} \underline{\underline{I}}$ , where

$$\alpha_{c/out} = 3\varepsilon_{out} \left( \frac{\varepsilon_c - \varepsilon_{out}}{\varepsilon_c + 2\varepsilon_{out}} \right). \quad (25)$$

## 4 Identically oriented dimers

If all dimers have the same orientation then the HCM is a uniaxial dielectric material [17, 18] with its distinguished axis parallel to the fixed unit vector  $\hat{\underline{d}}$ . That is,  $\underline{\underline{\varepsilon}}_{HCM}$  has the form given in Eq. (2).

### 4.1 Bruggeman formalism

Particles of all component materials are assumed as being immersed in the HCM itself, in the Bruggeman formalism [11, 12]. Thus, the expressions presented in §3.1 are appropriate here with the subscript ‘Br’ replacing the subscript ‘out’. The Bruggeman formalism rests on upon the assumption that the electric dipole moments arising from the electrically small spheres of the component materials, weighted by volume fraction, sum to the zero vector [22]; i.e.,

$$f_a \underline{p}_{dimer} + f_c \underline{p}_c = f_a (\underline{p}_a + \underline{p}_b) + f_c \underline{p}_c = \underline{0}. \quad (26)$$

Upon combining Eqs. (15)–(19) with Eq. (26), the dyadic equation

$$\begin{aligned} \underline{0} &= f_a \underline{\alpha}_{dimer/Br} + f_c \underline{\alpha}_{c/Br} \\ &= f_a \underline{\tilde{\alpha}}_{a/Br} + f_b \underline{\tilde{\alpha}}_{b/Br} + f_c \underline{\alpha}_{c/Br} \\ &= f_a \left[ \left( 1 - \sigma^2 \gamma^2 \alpha_{a/Br}^\perp \alpha_{b/Br}^\perp \right) \left( \underline{\underline{I}} - \hat{\underline{d}}\hat{\underline{d}} \right) + \left( 1 - 4\sigma^2 \alpha_{a/Br}^\parallel \alpha_{b/Br}^\parallel \right) \hat{\underline{d}}\hat{\underline{d}} \right]^{-1} \\ &\quad \cdot \left[ \left( \alpha_{a/Br}^\perp + \alpha_{b/Br}^\perp - 2\sigma\gamma \alpha_{a/Br}^\perp \alpha_{b/Br}^\perp \right) \left( \underline{\underline{I}} - \hat{\underline{d}}\hat{\underline{d}} \right) \right. \\ &\quad \left. + \left( \alpha_{a/Br}^\parallel + \alpha_{b/Br}^\parallel + 4\sigma \alpha_{a/Br}^\parallel \alpha_{b/Br}^\parallel \right) \hat{\underline{d}}\hat{\underline{d}} \right] \\ &\quad + f_c \left[ \alpha_{c/Br}^\perp \left( \underline{\underline{I}} - \hat{\underline{d}}\hat{\underline{d}} \right) + \alpha_{c/Br}^\parallel \hat{\underline{d}}\hat{\underline{d}} \right] \end{aligned} \quad (28)$$

emerges.

Due to the uniaxial symmetry, Eq. (28) represents two coupled scalar equations with  $\varepsilon_{Br}^\perp$  and  $\varepsilon_{Br}^\parallel$  as the two unknowns, which must be obtained by numerical methods. The following Jacobi scheme may be used for this purpose [24]. First, let us notice that  $\underline{\tilde{\alpha}}_{a,b/Br}$ , as defined in Eq. (16) (with the subscript ‘Br’ replacing the subscript ‘out’), may be written as

$$\left. \begin{aligned} \underline{\tilde{\alpha}}_{a/Br} &= \underline{\underline{M}}_b \cdot \underline{\alpha}_{a/Br} \\ \underline{\tilde{\alpha}}_{b/Br} &= \underline{\underline{M}}_a \cdot \underline{\alpha}_{b/Br} \end{aligned} \right\}, \quad (29)$$

wherein the  $3 \times 3$  dyadic

$$\begin{aligned} \underline{\underline{M}}_\ell &= \left\{ \underline{\underline{I}} - \sigma^2 \left[ \gamma^2 \left( \underline{\underline{I}} - \hat{\underline{\underline{d}}}\hat{\underline{\underline{d}}} \right) + 4 \hat{\underline{\underline{d}}}\hat{\underline{\underline{d}}} \right] \cdot \underline{\underline{\alpha}}_{a/Br} \cdot \underline{\underline{\alpha}}_{b/Br} \right\}^{-1} \\ &\quad \cdot \left\{ \underline{\underline{I}} + \sigma \left[ -\gamma \left( \underline{\underline{I}} - \hat{\underline{\underline{d}}}\hat{\underline{\underline{d}}} \right) + 2 \hat{\underline{\underline{d}}}\hat{\underline{\underline{d}}} \right] \cdot \underline{\underline{\alpha}}_{\ell/Br} \right\}, \quad \ell \in \{a, b\}. \end{aligned} \quad (30)$$

Second, notice that  $\underline{\underline{\alpha}}_{a,b,c/Br}$ , as defined in Eq. (5) (with the subscript ‘Br’ replacing the subscript ‘out’), may be written as

$$\underline{\underline{\alpha}}_{\ell/Br} = \left( \varepsilon_\ell \underline{\underline{I}} - \underline{\underline{\varepsilon}}_{Br} \right) \cdot \underline{\underline{P}}_\ell, \quad \ell \in \{a, b, c\}, \quad (31)$$

wherein the  $3 \times 3$  dyadic

$$\underline{\underline{P}}_\ell = \left[ \underline{\underline{I}} + i\omega \underline{\underline{D}}_{Br} \cdot \left( \varepsilon_\ell \underline{\underline{I}} - \underline{\underline{\varepsilon}}_{Br} \right) \right]^{-1}. \quad (32)$$

Hence, after using Eqs. (29) and (31), Eq. (27) may expressed as

$$f_a \left[ \underline{\underline{M}}_b \cdot \left( \varepsilon_a \underline{\underline{I}} - \underline{\underline{\varepsilon}}_{Br} \right) \cdot \underline{\underline{P}}_a + \underline{\underline{M}}_a \cdot \left( \varepsilon_b \underline{\underline{I}} - \underline{\underline{\varepsilon}}_{Br} \right) \cdot \underline{\underline{P}}_b \right] + f_c \left( \varepsilon_c - \underline{\underline{\varepsilon}}_{Br} \right) \cdot \underline{\underline{P}}_c = \underline{\underline{Q}}. \quad (33)$$

The Bruggeman estimate  $\underline{\underline{\varepsilon}}_{Br}$  may be extracted from Eq. (33) by the iterative scheme represented by

$$\underline{\underline{\varepsilon}}_{Br} = \mathcal{T} \left\{ \underline{\underline{\varepsilon}}_{Br} \right\}, \quad (34)$$

where the action of the dyadic operator  $\mathcal{T}$  is given by

$$\begin{aligned} \mathcal{T} \left\{ \underline{\underline{\varepsilon}}_{Br} \right\} &= \left[ f_a \left( \underline{\underline{M}}_b \cdot \underline{\underline{P}}_a + \underline{\underline{M}}_a \cdot \underline{\underline{P}}_b \right) + f_c \underline{\underline{P}}_c \right]^{-1} \\ &\quad \cdot \left[ f_a \left( \varepsilon_a \underline{\underline{M}}_b \cdot \underline{\underline{P}}_a + \varepsilon_b \underline{\underline{M}}_a \cdot \underline{\underline{P}}_b \right) + f_c \varepsilon_c \underline{\underline{P}}_c \right]. \end{aligned} \quad (35)$$

## 4.2 Maxwell Garnett formalism

Particles of component materials ‘a’ and ‘b’ are viewed as immersed in component material ‘c’, in the Maxwell Garnett formalism [11]. Thus, the expressions presented in §3.2 are appropriate here with the subscript ‘c’ replacing the subscript ‘out’. The electric dipole moments of spheres of component material ‘c’ are not relevant to this formalism, the HCM essentially arising as a perturbation of the component material ‘c’ by the addition of a relatively small amount of component materials ‘a’ and ‘b’. Consequently, results of the Maxwell Garnett formalism, as applied here, are strictly appropriate only for  $f_a \lesssim 0.15$ .

The Maxwell Garnett estimate of  $\underline{\underline{\varepsilon}}_{HCM}$  is obtained explicitly as [23]

$$\underline{\underline{\varepsilon}}_{MG} = \varepsilon_c \underline{\underline{I}} + f_a \left\{ \underline{\underline{\tilde{\alpha}}}_{a/c} \cdot \left[ \underline{\underline{I}} - \frac{2f_a}{3\varepsilon_c} \underline{\underline{\tilde{\alpha}}}_{a/c} \right]^{-1} + \underline{\underline{\tilde{\alpha}}}_{b/c} \cdot \left[ \underline{\underline{I}} - \frac{2f_a}{3\varepsilon_c} \underline{\underline{\tilde{\alpha}}}_{b/c} \right]^{-1} \right\}, \quad (36)$$

with the polarizability density dyadics  $\underline{\underline{\tilde{\alpha}}}_{a,b/c}$  as given in Eqs. (21).

## 5 Randomly oriented dimers

If the dimers are randomly oriented, the HCM is isotropic. Accordingly, the electrically small spheres of component materials ‘a’ and ‘b’ (and ‘c’ in the case of the Bruggeman formalism) should be regarded in this case as being immersed in an isotropic dielectric material and the expressions presented in §3.2 are appropriate.

Orientationally averaged electric dipole moments are defined as

$$\langle \underline{p}_\ell \rangle = \frac{1}{4\pi} \int_{\phi=0}^{2\pi} \int_{\theta=0}^{\pi} \underline{p}_\ell \sin \theta d\theta d\phi, \quad \ell \in \{a, b, c\}. \quad (37)$$

The orientationally averaged electric dipole moments for component materials ‘a’ and ‘b’ may be expressed as

$$\langle \underline{p}_\ell \rangle = \frac{4\pi}{3} s^3 \left( \frac{1}{4\pi} \int_{\phi=0}^{2\pi} \int_{\theta=0}^{\pi} \underline{\tilde{\alpha}}_{\ell/out} \sin \theta d\theta d\phi \right) \cdot \underline{E}_{inc}(\underline{Q}), \quad \ell \in \{a, b\}. \quad (38)$$

Herein the quantity in parenthesis represents the orientational average of the polarizability density dyadic  $\underline{\tilde{\alpha}}_{\ell/out}$ ; for later use, this is written as

$$\langle \underline{\tilde{\alpha}}_{\ell/out} \rangle = \tilde{\alpha}_{\ell/out}^{ave} \underline{I}, \quad \ell \in \{a, b\}. \quad (39)$$

Let us also note that

$$\left. \begin{aligned} \langle \underline{p}_{dimer} \rangle &= \langle \underline{p}_a \rangle + \langle \underline{p}_b \rangle \\ \langle \underline{\alpha}_{dimer/out} \rangle &= \langle \underline{\tilde{\alpha}}_{a/out} \rangle + \langle \underline{\tilde{\alpha}}_{b/out} \rangle \\ \alpha_{dimer/out}^{ave} &= \tilde{\alpha}_{a/out}^{ave} + \tilde{\alpha}_{b/out}^{ave} \end{aligned} \right\}. \quad (40)$$

Upon evaluating the integrals on the right side of Eq. (38), the following result is delivered:

$$\left. \begin{aligned} \langle \underline{p}_a \rangle &= \frac{4}{9} \pi s^3 \alpha_{a/out} \left[ \frac{2(1 - \sigma \alpha_{b/out})}{1 - \sigma^2 \alpha_{a/out} \alpha_{b/out}} + \frac{1 + 2\sigma \alpha_{b/out}}{1 - 4\sigma^2 \alpha_{a/out} \alpha_{b/out}} \right] \underline{E}_{inc}(\underline{Q}) \\ \langle \underline{p}_b \rangle &= \frac{4}{9} \pi s^3 \alpha_{b/out} \left[ \frac{2(1 - \sigma \alpha_{a/out})}{1 - \sigma^2 \alpha_{a/out} \alpha_{b/out}} + \frac{1 + 2\sigma \alpha_{a/out}}{1 - 4\sigma^2 \alpha_{a/out} \alpha_{b/out}} \right] \underline{E}_{inc}(\underline{Q}) \end{aligned} \right\}. \quad (41)$$

In the special case of homodimers,  $\underline{p}_a = \underline{p}_b$  and the corresponding orientationally averaged electric dipole moment is given as

$$\langle \underline{p}_a \rangle = \langle \underline{p}_b \rangle = \frac{4}{3} \pi s^3 \alpha_{a/out} \left[ \frac{\tilde{\sigma} - 1}{(\tilde{\sigma} + 1)(2\tilde{\sigma} - 1)} \right] \underline{E}_{inc}(\underline{Q}). \quad (42)$$

Since spheres of material ‘c’ have no directional dependency, the orientational average of the associated electric dipole moment is simply  $\underline{p}_c$  itself; i.e.,

$$\langle \underline{p}_c \rangle = \frac{4}{3} \pi s^3 \alpha_{c/out} \underline{E}_{inc}(\underline{Q}). \quad (43)$$

## 5.1 Bruggeman formalism

In the Bruggeman formalism, particles of all component materials are assumed as being immersed in the HCM itself. Thus, the expressions presented in §3.2 can be used here with the subscript ‘out’ replaced by the subscript ‘Br’. The Bruggeman formalism dictates that

$$f_a \langle \underline{p}_{dimer} \rangle + f_c \langle \underline{p}_c \rangle = f_a \left( \langle \underline{p}_a \rangle + \langle \underline{p}_b \rangle \right) + f_c \langle \underline{p}_c \rangle = \underline{0}. \quad (44)$$

Upon combining Eqs. (41) and (43) with Eq. (44), the corresponding scalar Bruggeman equation emerges as

$$\begin{aligned} & f_a \left\{ \frac{\alpha_{a/Br}}{3} \left[ \frac{2(1 - \sigma \alpha_{b/Br})}{1 - \sigma^2 \alpha_{a/Br} \alpha_{b/Br}} + \frac{1 + 2\sigma \alpha_{b/Br}}{1 - 4\sigma^2 \alpha_{a/Br} \alpha_{b/Br}} \right] \right. \\ & \left. + \frac{\alpha_{b/Br}}{3} \left[ \frac{2(1 - \sigma \alpha_{a/Br})}{1 - \sigma^2 \alpha_{a/Br} \alpha_{b/Br}} + \frac{1 + 2\sigma \alpha_{a/Br}}{1 - 4\sigma^2 \alpha_{a/Br} \alpha_{b/Br}} \right] \right\} + f_c \alpha_{c/Br} = 0. \end{aligned} \quad (45)$$

After using Eqs. (14), (20), and (25) to substitute for  $\sigma$ ,  $\alpha_{a,b/Br}$ , and  $\alpha_{c/Br}$ , respectively, Eq. (45) may be recast as a quintic polynomial in  $\varepsilon_{Br}$ . (In the case of homodimers, this polynomial reduces to a cubic polynomial in  $\varepsilon_{Br}$ ). A Jacobi numerical scheme [24] can be used to extract  $\varepsilon_{Br}$  from Eq. (45). That is, the solution may be found using the iterative scheme represented by

$$\varepsilon_{Br} = \mathcal{S} \{ \varepsilon_{Br} \}, \quad (46)$$

where the action of the scalar operator  $\mathcal{S}$  is given by

$$\mathcal{S} \{ \varepsilon_{Br} \} = \frac{\frac{m_b \varepsilon_a}{\varepsilon_a + 2\varepsilon_{Br}} + \frac{m_a \varepsilon_b}{\varepsilon_b + 2\varepsilon_{Br}} + \frac{f_c \varepsilon_c}{\varepsilon_c + 2\varepsilon_{Br}}}{\frac{m_b}{\varepsilon_a + 2\varepsilon_{Br}} + \frac{m_a}{\varepsilon_b + 2\varepsilon_{Br}} + \frac{f_c}{\varepsilon_c + 2\varepsilon_{Br}}}, \quad (47)$$

with the scalar parameters

$$\left. \begin{aligned} m_a &= \frac{f_a}{3} \left[ \frac{2(1 - \sigma\alpha_{a/Br})}{1 - \sigma^2\alpha_{a/Br}\alpha_{b/Br}} + \frac{1 + 2\sigma\alpha_{a/Br}}{1 - 4\sigma^2\alpha_{a/Br}\alpha_{b/Br}} \right] \\ m_b &= \frac{f_a}{3} \left[ \frac{2(1 - \sigma\alpha_{b/Br})}{1 - \sigma^2\alpha_{a/Br}\alpha_{b/Br}} + \frac{1 + 2\sigma\alpha_{b/Br}}{1 - 4\sigma^2\alpha_{a/Br}\alpha_{b/Br}} \right] \end{aligned} \right\}. \quad (48)$$

## 5.2 Maxwell Garnett formalism

In the Maxwell Garnett formalism, particles of component materials ‘a’ and ‘b’ are viewed as immersed in component material ‘c’. Accordingly, here the expressions presented in §3.2 are used with the subscript ‘c’ replacing the subscript ‘out’. The Maxwell Garnett estimate of  $\varepsilon_{HCM}$  is given explicitly by

$$\varepsilon_{MG} = \varepsilon_c \left\{ 1 + 3f_a \left[ \frac{\tilde{\alpha}_{a/c}^{ave}}{3\varepsilon_c - 2f_a\tilde{\alpha}_{a/c}^{ave}} + \frac{\tilde{\alpha}_{b/c}^{ave}}{3\varepsilon_c - 2f_a\tilde{\alpha}_{b/c}^{ave}} \right] \right\}, \quad (49)$$

where

$$\left. \begin{aligned} \tilde{\alpha}_{a/c}^{ave} &= \frac{1}{3}\alpha_{a/c} \left[ \frac{2(1 - \sigma\alpha_{b/c})}{1 - \sigma^2\alpha_{a/c}\alpha_{b/c}} + \frac{1 + 2\sigma\alpha_{b/c}}{1 - 4\sigma^2\alpha_{a/c}\alpha_{b/c}} \right] \\ \tilde{\alpha}_{b/c}^{ave} &= \frac{1}{3}\alpha_{b/c} \left[ \frac{2(1 - \sigma\alpha_{a/c})}{1 - \sigma^2\alpha_{a/c}\alpha_{b/c}} + \frac{1 + 2\sigma\alpha_{a/c}}{1 - 4\sigma^2\alpha_{a/c}\alpha_{b/c}} \right] \end{aligned} \right\}. \quad (50)$$

## 6 Numerical results

Let us now present representative numerical results based on the theoretical results established in §2–§5. Although the range  $f_a \in [0, 0.5]$  may appear appropriate at first glance, the maximum value of  $f_a$  must be less than 0.5. This is because no sphere of material ‘c’ must be allowed to occupy the region between the two spheres constituting a dimer. Nevertheless, we have provided the Bruggeman estimates for  $f_a \in [0, 0.5]$ , because the upper limit of  $f_a$  will have to be decided experimentally for a specific composite material. The Maxwell Garnett formalism is appropriate only for dilute composite materials, and we have restricted the presentation of the Maxwell Garnett estimates to  $f_a \in [0, 0.15]$ .

### 6.1 Dielectric–dielectric dimers

Suppose, first, that both component materials ‘a’ and ‘b’ are nondissipative dielectric materials, specified by the permittivities  $\varepsilon_a = 2\varepsilon_0$  and  $\varepsilon_b \in (\varepsilon_0, 10\varepsilon_0)$ . The dielectric–dielectric dimers which arise from the combination of component materials ‘a’ and ‘b’ are randomly dispersed along with component material ‘c’ specified by the permittivity  $\varepsilon_c = (14 + 4i)\varepsilon_0$ .

### 6.1.1 Randomly oriented dimers

The real and imaginary parts of  $\varepsilon_{MG}/\varepsilon_0$  and  $\varepsilon_{Br}/\varepsilon_0$  are plotted against  $\varepsilon_b/\varepsilon_0$  and  $f_a$  in Fig. 1, for the case where the dimers are randomly oriented and  $d = 2s$ . The real part of  $\varepsilon_{MG}$  decreases approximately linearly as  $f_a$  increases, with its rate of decrease being greatest at the lowest values of  $\varepsilon_b$ . Furthermore, the real part of  $\varepsilon_{MG}$  increases approximately linearly as  $\varepsilon_b$  increases, with its rate of increase being greatest at the largest values of  $f_a$ . The imaginary part of  $\varepsilon_{MG}$  decreases approximately linearly as  $f_a$  increases, and this trend is almost independent of the value of  $\varepsilon_b$ . For the range  $0 < f_a \lesssim 0.15$ , the real and imaginary parts of  $\varepsilon_{Br}$  are very similar, both qualitatively and quantitatively, to the real and imaginary parts of  $\varepsilon_{MG}$ . For  $f_a \gtrsim 0.15$ , both the real and imaginary parts of  $\varepsilon_{Br}$  exhibit a more nonlinear dependency on  $f_a$  than they do at lower values of  $f_a$ .

The issue of the influence of the dimer separation distance upon  $\varepsilon_{HCM}$  is addressed via Fig. 2, wherein the real and imaginary parts of  $\varepsilon_{MG}/\varepsilon_0$  and  $\varepsilon_{Br}/\varepsilon_0$  are plotted against  $d/s$  for  $\varepsilon_b = \varepsilon_0$  (green, solid curves),  $2\varepsilon_0$  (blue, dashed curves), and  $3\varepsilon_0$  (red, broken dashed curves), when  $f_a = 0.15$ . The influence of  $d$  on the real and imaginary parts of  $\varepsilon_{HCM}$ , for both the Bruggeman and Maxwell Garnett estimates, decays rapidly as  $d$  increases. Indeed, both estimates of  $\varepsilon_{HCM}$  are practically independent of  $d$  for  $d > 4s$ , these estimates being essentially the same as those that would be obtained through the homogenization of three independent component materials ‘a’, ‘b’, and ‘c’ with no dimeric interaction between the spheres of component materials ‘a’ and ‘b’. The change in the real part of  $\varepsilon_{MG}$  as  $d$  increases from zero to  $4s$  is approximately 0.2%, whereas the corresponding change in the imaginary part of  $\varepsilon_{MG}$  is approximately 0.4%. The Bruggeman estimates of  $\varepsilon_{HCM}$  are somewhat more sensitive to changes in  $d$ , the real part of  $\varepsilon_{Br}$  changing by approximately 1.6% whereas the imaginary part of  $\varepsilon_{Br}$  changing by approximately 2.8% as  $d$  increases from zero to  $4s$ .

### 6.1.2 Identically oriented dimers

Qualitatively, the Bruggeman and Maxwell Garnett estimates of  $\varepsilon_{HCM}^{\parallel}$  and  $\varepsilon_{HCM}^{\perp}$  for composite materials containing identically oriented dimers have dependencies similar to the estimates of  $\varepsilon_{HCM}$  presented in Figs. 1 and 2 for composite materials containing randomly oriented dimers. This becomes evident from the plots of the averages  $(\varepsilon_{MG}^{\parallel} + \varepsilon_{MG}^{\perp})/2\varepsilon_0$  and  $(\varepsilon_{Br}^{\parallel} + \varepsilon_{Br}^{\perp})/2\varepsilon_0$  with respect to  $\varepsilon_b/\varepsilon_0$  and  $f_a$  in Fig. 3. To the naked eye, the plots in Figs. 1 and 3 are almost indistinguishable.

However, there are significant quantitative differences between the estimates of  $\varepsilon_{HCM}^{\parallel}$  and  $\varepsilon_{HCM}^{\perp}$ . In Fig. 4, the real and imaginary parts of the differences  $(\varepsilon_{MG}^{\parallel} - \varepsilon_{MG}^{\perp})/\varepsilon_0$  and  $(\varepsilon_{Br}^{\parallel} - \varepsilon_{Br}^{\perp})/\varepsilon_0$  are plotted against  $\varepsilon_b/\varepsilon_0$  and  $f_a$ , when  $d = 2s$ . Both the real and imaginary parts of the difference  $\varepsilon_{MG}^{\parallel} - \varepsilon_{MG}^{\perp}$  increase approximately linearly as  $f_a$  increases and decrease approximately linearly as  $\varepsilon_b$  increases. Thus, the greatest degree of anisotropy is predicted by the Maxwell Garnett formalism when  $f_a$  is largest and  $\varepsilon_b$  is smallest.

In the range  $0 < f_a \lesssim 0.15$ , both the real and imaginary parts of the difference  $\varepsilon_{Br}^{\parallel} - \varepsilon_{Br}^{\perp}$  are qualitatively similar to the corresponding real and imaginary parts of  $\varepsilon_{MG}^{\parallel} - \varepsilon_{MG}^{\perp}$ . However, at larger values of  $f_a$ , both the real and imaginary parts of  $\varepsilon_{Br}^{\parallel} - \varepsilon_{Br}^{\perp}$  exhibit strong nonlinear dependencies on  $f_a$ . The greatest degree of anisotropy is predicted by the Bruggeman formalism to be in the vicinity of  $f_a \approx 0.2$  with  $\varepsilon_b = \varepsilon_0$ . Broadly, over the parameter ranges considered, the degree of anisotropy estimated by the Maxwell Garnett formalism is slightly larger than that estimated by the Bruggeman formalism.

The degree of anisotropy exhibited by the HCM, as estimated by the Bruggeman and Maxwell Garnett formalisms, decays rapidly as the separation distance  $d$  in the dimer increases. This is illustrated in Fig. 5 wherein the real and imaginary parts of the differences  $(\varepsilon_{MG}^{\parallel} - \varepsilon_{MG}^{\perp})/\varepsilon_0$  and  $(\varepsilon_{Br}^{\parallel} - \varepsilon_{Br}^{\perp})/\varepsilon_0$  are plotted against  $d/s$  for  $\varepsilon_b = \varepsilon_0$  (green, solid curves),  $2\varepsilon_0$  (blue, dashed curves), and  $3\varepsilon_0$  (red, broken dashed curves). Here  $f_a = 0.15$ . The graphs for  $\varepsilon_{Br}^{\parallel} - \varepsilon_{Br}^{\perp}$  and  $\varepsilon_{MG}^{\parallel} - \varepsilon_{MG}^{\perp}$  in Fig. 5 are qualitatively similar, with the Maxwell Garnett estimates being slightly larger than the Bruggeman estimates at each value of  $d$  and  $\varepsilon_b$ . The degree of anisotropy, as estimated by both formalisms, falls most rapidly for the smallest value of  $\varepsilon_b$ . Furthermore, the degree of anisotropy, as estimated by both formalisms, vanishes almost entirely at  $d = 4s$ .

## 6.2 Metal–dielectric dimers

Next, suppose that component material ‘a’ is a metal. For definiteness, this metal is taken to be silver as characterized by the size-dependent permittivity [25, 26]

$$\varepsilon_{Ag}(s) = \varepsilon_0 \left[ 1 - \frac{\omega_p^2}{\omega^2 + i\omega \left( \gamma_{Ag} + \frac{3v_F}{4s} \right)} \right]. \quad (51)$$

Herein,  $v_F = 1.4 \times 10^6 \text{ m s}^{-1}$  is the electron speed at the Fermi surface,  $\gamma_{Ag} = 10^{14} \text{ s}^{-1}$  is the relaxation rate, and  $\omega_p = 1.38 \times 10^{16} \text{ rad s}^{-1}$  is the plasma frequency. The angular frequency is  $\omega = 2\pi c_0/\lambda_0$ , with the free-space wavelength chosen to be  $\lambda_0 = 650 \text{ nm}$ . As in §6.1, component material ‘b’ is a nondissipative dielectric material specified by the permittivity  $\varepsilon_b \in (\varepsilon_0, 10\varepsilon_0)$ . The metal–dielectric dimers which arise from the combination of component materials ‘a’ and ‘b’ are randomly mixed with component material ‘c’ which is specified by the permittivity  $\varepsilon_c = (14 + 4i)\varepsilon_0$  for all results presented here.

### 6.2.1 Randomly oriented dimers

For composite materials containing randomly oriented dimers, the real and imaginary parts of  $\varepsilon_{MG}/\varepsilon_0$  and  $\varepsilon_{Br}/\varepsilon_0$  are plotted in Fig. 6 against  $\varepsilon_b/\varepsilon_0$  and  $f_a$  for  $d = 2s$  and  $s = 5 \text{ nm}$ . Thus,  $\varepsilon_a = (-21.4 + 2.4i)\varepsilon_0$  by virtue of Eq. (51). The graphs of the real parts of  $\varepsilon_{MG}$  and  $\varepsilon_{Br}$  in Fig. 6 are qualitatively similar to the corresponding graphs in Fig. 1 for dielectric–dielectric dimers. In contrast, graphs of the imaginary parts of  $\varepsilon_{MG}$  and  $\varepsilon_{Br}$  in Fig. 6 are rather different to the corresponding graphs in Fig. 1, both qualitatively and quantitatively. On the whole, the imaginary parts of  $\varepsilon_{MG}$  and  $\varepsilon_{Br}$  are substantially larger in Fig. 6 than they are in Fig. 1. Furthermore, the imaginary parts of  $\varepsilon_{MG}$  and  $\varepsilon_{Br}$  in Fig. 6 are substantially more nonlinear with respect to increasing  $f_a$  than are the corresponding quantities in Fig. 1. Both the real and imaginary parts of  $\varepsilon_{MG}$  and  $\varepsilon_{Br}$  are qualitatively similar in Fig. 6 in the range  $0 < f_a \lesssim 0.15$ . However, across this range, the quantitative differences between the estimates  $\varepsilon_{MG}$  and  $\varepsilon_{Br}$  are substantially larger than the corresponding differences presented in Fig. 1, and these differences between  $\varepsilon_{MG}$  and  $\varepsilon_{Br}$  grow as  $f_a$  increases from zero.

Qualitatively, the influence of the dimer separation distance  $d$  upon  $\varepsilon_{HCM}$  for the metal–dielectric dimer HCM is similar to that for the dielectric–dielectric dimer HCM. This may be appreciated by comparing Fig. 2 with Fig. 7. In Fig. 7, the real and imaginary parts of  $\varepsilon_{MG}/\varepsilon_0$  and  $\varepsilon_{Br}/\varepsilon_0$  are plotted against  $d/s$  for  $\varepsilon_b = \varepsilon_0$  (green, solid curves),  $2\varepsilon_0$  (blue, dashed curves), and  $3\varepsilon_0$  (red, broken dashed curves), for the metal–dielectric dimer HCM, with  $f_a = 0.02$  and  $s = 5 \text{ nm}$ . As is the case for dielectric–dielectric dimers in Fig. 2, the estimates of  $\varepsilon_{HCM}$  for metal–dielectric dimers in Fig. 7 are practically independent of  $d$  for  $d > 4s$ . The magnitudes of the relative changes in  $\varepsilon_{HCM}$  as  $d$  increases from zero to  $4s$  in Fig. 7 are similar to those in Fig. 2, with the Bruggeman estimates being somewhat more sensitive than the Maxwell Garnett estimates to changes in  $d$ .

The effects of the size of the metal particles which make up component material ‘a’ are delineated in Fig. 8. Herein the real and imaginary parts of  $\varepsilon_{MG}/\varepsilon_0$  and  $\varepsilon_{Br}/\varepsilon_0$  are plotted against  $s$  for  $\varepsilon_b = \varepsilon_0$  (green, solid curves),  $2\varepsilon_0$  (blue, dashed curves), and  $3\varepsilon_0$  (red, broken dashed curves), with  $f_a = 0.02$  and  $d = 2s$ . The influence of  $s$  on the real and imaginary parts of  $\varepsilon_{HCM}$ , for both the Bruggeman and Maxwell Garnett estimates, decays rapidly as  $s$  increases. Indeed, the estimates of  $\varepsilon_{HCM}$  vary little as  $s$  increases beyond 20 nm. The change in the real part of  $\varepsilon_{MG}$  as  $s$  increases from 5 to 20 nm is approximately 2.6%, whereas the corresponding change in the imaginary part of  $\varepsilon_{MG}$  is approximately 1.0%. The real part of  $\varepsilon_{Br}$  changes by approximately 1.2% whereas the imaginary part of  $\varepsilon_{Br}$  changes by approximately 1.8%, as  $s$  increases from 5 to 20 nm. Most strikingly, the real and imaginary parts of  $\varepsilon_{MG}$ , as well as the real part of  $\varepsilon_{Br}$ , uniformly decrease as  $s$  increases from 5 to 20 nm whilst the imaginary part of  $\varepsilon_{Br}$  uniformly increases as  $s$  increases.

### 6.2.2 Identically oriented dimers

The estimates of  $\varepsilon_{HCM}^{\parallel}$  and  $\varepsilon_{HCM}^{\perp}$  yielded by the Bruggeman and Maxwell Garnett formalisms for composite materials containing identically oriented dimers exhibit characteristics that are qualitatively similar to those displayed in Figs. 6–8 by the corresponding estimates of  $\varepsilon_{HCM}$  for randomly oriented dimers. However, significant quantitative differences arise between the estimates of  $\varepsilon_{HCM}^{\parallel}$  and  $\varepsilon_{HCM}^{\perp}$ . The real and imaginary parts of the differences  $(\varepsilon_{MG}^{\parallel} - \varepsilon_{MG}^{\perp})/\varepsilon_0$  and  $(\varepsilon_{Br}^{\parallel} - \varepsilon_{Br}^{\perp})/\varepsilon_0$  are plotted in Fig. 9 against  $\varepsilon_b/\varepsilon_0$  and  $f_a$ , for  $d = 2s$  and  $s = 5$  nm. Across the range  $0 < f_a \lesssim 0.15$ , the differences  $\varepsilon_{HCM}^{\parallel} - \varepsilon_{HCM}^{\perp}$  estimated by the Maxwell Garnett and Bruggeman formalisms are qualitatively similar. However, there are quantitative differences between  $\varepsilon_{Br}^{\parallel} - \varepsilon_{Br}^{\perp}$  and  $\varepsilon_{MG}^{\parallel} - \varepsilon_{MG}^{\perp}$ , and these increase in magnitude as  $f_a$  increases. The greatest degree of anisotropy is estimated by the Bruggeman formalism to exist when both  $f_a$  and  $\varepsilon_b$  are maximum. In contrast, the greatest degree of anisotropy is estimated by the Maxwell Garnett formalism to exist when  $f_a$  is maximum but  $\varepsilon_b$  is minimum.

The influences of the dimer separation distance  $d$  and the metal sphere radius  $s$  upon the anisotropy of the HCM are delineated in Fig. 10. Here the real and imaginary parts of the differences  $(\varepsilon_{MG}^{\parallel} - \varepsilon_{MG}^{\perp})/\varepsilon_0$  and  $(\varepsilon_{Br}^{\parallel} - \varepsilon_{Br}^{\perp})/\varepsilon_0$  are plotted against  $s$  (in nm) and  $d/s$ , for  $f_a = 0.02$  and  $d = 2s$ . While the real part of  $\varepsilon_{MG}^{\parallel} - \varepsilon_{MG}^{\perp}$  decreases uniformly as  $d$  increases from  $2s$  to  $4s$ , this quantity varies very little as  $s$  increases from 5 nm to 20 nm. The imaginary part of  $\varepsilon_{MG}^{\parallel} - \varepsilon_{MG}^{\perp}$  increases uniformly as  $d$  increases from  $2s$  to  $4s$ ; in contrast, the imaginary part of  $\varepsilon_{MG}^{\parallel} - \varepsilon_{MG}^{\perp}$  varies only marginally as  $s$  increases from 5 nm to 20 nm. The graphs for the real and imaginary parts of  $\varepsilon_{Br}^{\parallel} - \varepsilon_{Br}^{\perp}$  are both qualitatively and quantitatively similar to the corresponding graphs for  $\varepsilon_{MG}^{\parallel} - \varepsilon_{MG}^{\perp}$ .

## 7 Discussion

The Bruggeman and Maxwell Garnett formalisms have been established in the preceding sections for the homogenization of composite materials containing randomly oriented and identically oriented dimers. The representative numerical results presented in §6.1 for the case of dielectric–dielectric dimers demonstrate close agreement between the estimates of the HCM constitutive parameters delivered by the Bruggeman and Maxwell Garnett formalisms for both randomly oriented and identically oriented dimers. The Bruggeman formalism is advantageous over the Maxwell Garnett formalism insofar as the former is appropriate for arbitrary dimer volume fractions whereas the latter is appropriate only for low dimer volume fractions. On the other hand, the Maxwell Garnett formalism is relatively straightforward to implement numerically as its estimates are provided as explicit formulas, in contrast to the Bruggeman formalism whose numerical implementation typically involves the iterative extraction of estimates from implicit formulas.

The case of metal–dielectric dimers should generally be approached with caution. If attention is restricted to parameter regimes involving low dimer volume fractions and moderate degrees of dissipation then, as demonstrated in §6.2, the Bruggeman and Maxwell Garnett formalisms deliver estimates of the HCM constitutive parameters which are in broad agreement. However, at higher dimer volume fractions, substantial qualitative and quantitative differences emerge between the estimates provided by the two formalisms, and these differences are exacerbated by anisotropy in the case of identically oriented dimers.

The difficulties that arise for metal–dielectric dimers at larger values of the dimer volume fraction essentially stem from the fact the real part of  $\varepsilon_a$  is negative while the real parts of  $\varepsilon_{b,c}$  are positive. In the absence of substantial degrees of dissipation, homogenization for such parameter regimes can be problematic for conventional formalisms, especially at mid-range values of volume fractions [27, 28, 29, 30]. For examples, in these parameter regimes the Bruggeman estimates may violate the Hashin–Shtrikman bounds, and the Maxwell Garnett estimates may exhibit very large resonances (with respect to varying volume fraction). These issues affect both passive and active HCMs [31], for both forward and inverse homogenization formalisms [32], and also impose limitations on the Bergman–Milton bounds [33].

The mathematical origin of these problematic parameter regimes may be appreciated most readily by considering the simplest case, namely that of randomly oriented homodimers. The corresponding expression for the orientationally averaged electric dipole moment is provided in Eq. (42). The polarizability scalar  $\alpha_{a/out}$  therein becomes infinitely large in magnitude in the limit  $\varepsilon_a \rightarrow -2\varepsilon_{out}$ . This eventuality — which is sometimes referred to as a Fröhlich mode [25] — may result in singular or highly resonant behavior in the estimates of HCM permittivity. There is further scope for singular behavior which is solely attributable to the dimer interaction: the denominator term in Eq. (42) is null valued at  $\tilde{\sigma} \in \{-1, 1/2\}$ . By using the definition of  $\tilde{\sigma}$  provided in Eq. (24) with  $d = 2s$ , these singularities arise in the limits  $\varepsilon_a \rightarrow -(17/7)\varepsilon_{out}$  and  $\varepsilon_a \rightarrow -3\varepsilon_{out}$ , respectively. For strictly nondissipative materials, the possibility of  $\varepsilon_a/\varepsilon_{out} \in \{-2, -(17/7), -3\}$  can only arise if either  $\varepsilon_a\varepsilon_b < 0$  or  $\varepsilon_a\varepsilon_c < 0$ . Thus, by extrapolation, it may be anticipated that regimes in which the real part of  $\varepsilon_a$  is negative while the real parts of at least one of  $\varepsilon_b$  or  $\varepsilon_c$  is positive may well be problematic. However, as demonstrated in §6.2, provided that only low dimer volume fractions are considered and there is a moderate degree of dissipation, the problems of singular or highly resonant behavior may not arise.

The numerical results in §6 reveal that the effects of intradimer coupling decay rapidly as  $d$  increases. Indeed, for  $d > 4s$  these effects are generally negligible and the permittivity dyadic of the HCM is practically the same as that which would arise in the case where component materials ‘a’ and ‘b’ were not coupled at all. By comparing the numerical results at  $d = 2s$  with those at  $d = 4s$  in Figs. 2, 5, 7, and 10, it may be deduced that intradimer coupling generally has relatively modest but not insignificant effects on the HCM parameter estimates delivered by the Bruggeman and Maxwell Garnett formalisms, and that these effects are exacerbated by anisotropy in the case of identically oriented dimers.

**Acknowledgement.** AL thanks the Charles Godfrey Binder Endowment at Penn State for ongoing support of his research activities.

## References

- [1] Schulz MJ, Kelkar AD, Sundaresan MJ. Nanoengineering of structural, functional and smart materials. London (UK): CRC Press; 2005.
- [2] Lombardi A, Grzelczak MP, Crut A, Maioli P, Pastoriza-Santos I, Liz-Marzán LM, Del Fatti N, Vallée F. Optical response of individual Au-Ag@SiO<sub>2</sub> heterodimers. ACS Nano 2013; 7:2522–2531.
- [3] Park W. Optical interactions in plasmonic nanostructures. Nano Convergence 2014; 1:2.
- [4] Marinica DC, Kazansky AK, Nordlander P, Aizpurua J, Borisov AG. Quantum plasmonics: nonlinear effects in the field enhancement of a plasmonic nanoparticle dimer. Nano Lett. 2012; 12:1333–1339.
- [5] Okazaki R, Ikemoto Y, Moriwaki T, Shikama T, Takahashi K, Mori H, Nakaya H, Sasaki T, Yasui Y, Terasaki I. Optical conductivity measurement of a dimer Mott-insulator to charge-order phase transition in a two-dimensional quarter-filled organic salt compound. Phys. Rev. Lett. 2013; 111:217801.
- [6] Chen R, Lee SB, Balents L. Dimer Mott insulator in an oxide heterostructure. Phys. Rev. B 2013; 87:161119.
- [7] Gupta SK, Singh DP, Manohar R, Hiremath US, Yelmaggad CV. Dielectric behaviour of a ferroelectric liquid crystal dimer. Liquid Crystals 2012; 39:1125–1129.
- [8] Šljivančanin Ž, Rauls E, Hornekær L, Xu W, Besenbacher F, Hammer B. Extended atomic hydrogen dimer configurations on the graphite(0001) surface. J. Chem. Phys. 2009; 131:084706.
- [9] Zhang F, Sadaune V, Kang L, Zhao Q, Zhou J, Lippens D. Coupling effect for dielectric metamaterial dimer. Prog. Electromag. Res. 2012; 132:587–601.

- [10] Kim IC, Torquato S. Effective conductivity of suspensions of overlapping spheres. *J. Appl. Phys.* 1992; 71:2727–2735.
- [11] Lakhtakia A (ed.). Selected papers on linear optical composite materials. Bellingham (WA): SPIE Optical Engineering Press; 1996.
- [12] Mackay TG, Lakhtakia A. Electromagnetic fields in linear bianisotropic mediums. *Prog. Opt.* 2008; 51:121–209.
- [13] Tsang L, Kong JA. Scattering of electromagnetic waves from random media with strong permittivity fluctuations. *Radio Sci.* 1981; 16:303–320.
- [14] Faxén H. Der Zusammenhang zwischen den Maxwellschen Gleichungen für Dielektrika und den atomistischen Ansätzen von H. A. Lorentz u.a. *Zeit. Phys.* 1920; 2:218–229.
- [15] Lakhtakia A. Size-dependent Maxwell-Garnett formula from an integral equation formalism. *Optik* 1992; 91:134–137.
- [16] Hashin Z, Shtrikman S. A variational approach to the theory of the effective magnetic permeability of multiphase materials. *J. Appl. Phys.* 1962; 33:3125–3131.
- [17] Chen HC. Theory of electromagnetic waves. New York (NY): McGraw–Hill; 1983.
- [18] Mackay TG, Lakhtakia A. Electromagnetic anisotropy and bianisotropy. Singapore: World Scientific; 2010.
- [19] Jackson JD. Classical electrodynamics, 3rd edn. New York (NY): Wiley; 1999.
- [20] Michel B. A Fourier space approach to the pointwise singularity of an anisotropic dielectric medium. *Int. J. Appl. Electromagn. Mech.* 1997; 8:219–227.
- [21] Weiglhofer WS, Lakhtakia A, Monzon JC. Maxwell–Garnett model for composites of electrically small uniaxial objects. *Microw. Opt. Technol. Lett.* 1993; 6:681–684.
- [22] Ross BM, Lakhtakia A. Bruggeman approach for isotropic chiral mixtures revisited. *Microw. Opt. Technol. Lett.* 2005; 44:524–527.
- [23] Weiglhofer WS, Lakhtakia A, Michel B. Maxwell Garnett and Bruggeman formalisms for a particulate composite with bianisotropic host medium. *Microw. Opt. Technol. Lett.* 1997; 15:263–266. Corrections: 1999; 22:221.
- [24] Rao SS. Applied numerical methods for engineers and scientists. Cambridge (UK): Pearson Publishing; 2001.
- [25] Bohren CF, Huffman DR. Absorption and scattering of light by small particles. New York (NY): Wiley; 1983.
- [26] Kreibig U. Electronic properties of small silver particles: the optical constants and their temperature dependence. *J. Phys. F: Metal Phys.* 1974; 4:999–1014.
- [27] Mackay TG, Lakhtakia A. A limitation of the Bruggeman formalism for homogenization. *Opt. Commun.* 2004; 234:35–42. Corrections: 2009; 282:4028.
- [28] Mackay TG. On the effective permittivity of silver–insulator nanocomposites. *J. Nanophoton.* 2007; 1:019501.
- [29] Fourn C, Brosseau C. Electrostatic resonances of heterostructures with negative permittivity: Homogenization formalisms versus finite-element modeling. *Phys. Rev. E* 2008; 77:016603.

- [30] Mejdoubi A, Brosseau C. Electrostatic resonance of clusters of dielectric cylinders: A finite element simulation. *Phys. Lett. A* 2008; 372:741–748.
- [31] Mackay TG, Lakhtakia A. On the application of homogenization formalisms to active dielectric composite materials. *Opt. Commun.* 2009; 282:2470–2475.
- [32] Jamaian SS, Mackay TG. On limitations of the Bruggeman formalism for inverse homogenization. *J. Nanophoton.* 2010; 4:043510.
- [33] Duncan AJ, Mackay TG, Lakhtakia A. On the Bergman–Milton bounds for the homogenization of dielectric composite materials. *Opt. Commun.* 2007; 271:470–474.

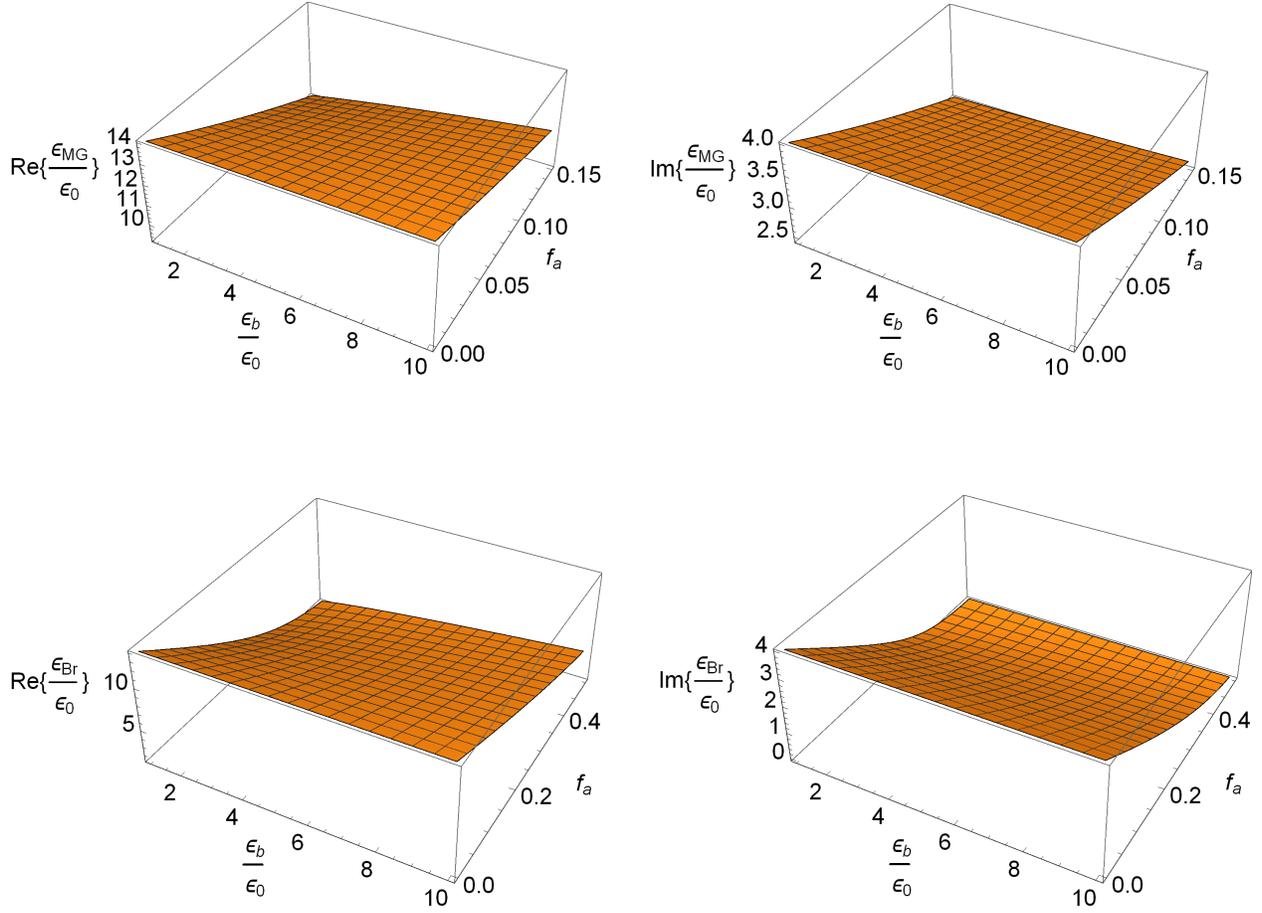


Figure 1: The real and imaginary parts of  $\epsilon_{MG}/\epsilon_0$  and  $\epsilon_{Br}/\epsilon_0$  plotted against  $\epsilon_b/\epsilon_0$  and  $f_a$  for the case where the electrically small spheres of component materials ‘a’ and ‘b’ combine to form dielectric–dielectric dimers with  $\epsilon_a = 2\epsilon_0$  and  $\epsilon_b \in (1, 10)\epsilon_0$ . Component material ‘c’ is specified by  $\epsilon_c = (14 + 4i)\epsilon_0$ . The dimers are randomly oriented and  $d = 2s$ .

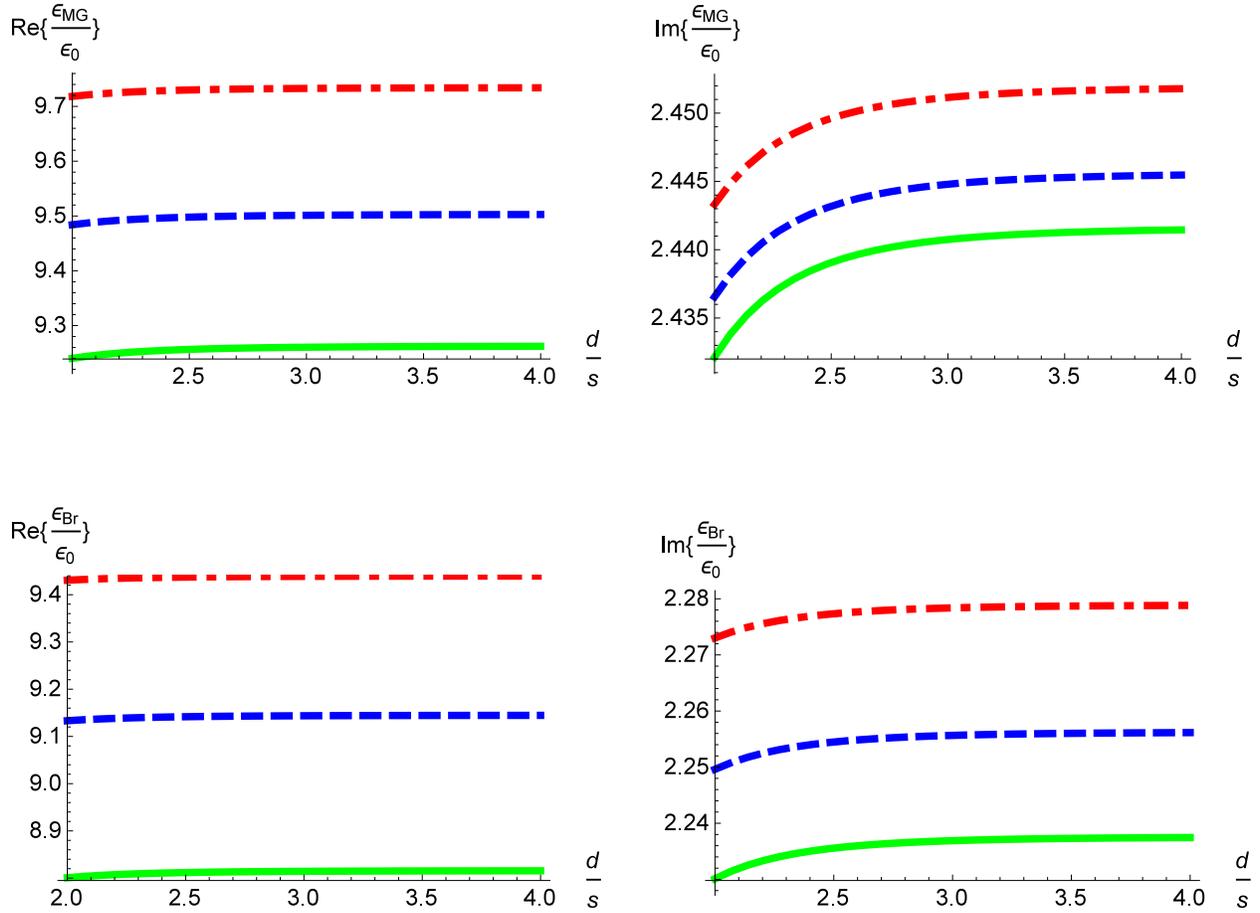


Figure 2: As Fig. 1 except that the real and imaginary parts of  $\epsilon_{MG}/\epsilon_0$  and  $\epsilon_{Br}/\epsilon_0$  are plotted against  $d/s$  for  $\epsilon_a = 2\epsilon_0$  and  $\epsilon_b = \epsilon_0$  (green, solid curves),  $2\epsilon_0$  (blue, dashed curves), and  $3\epsilon_0$  (red, broken dashed curves). Here  $f_a = 0.15$ .

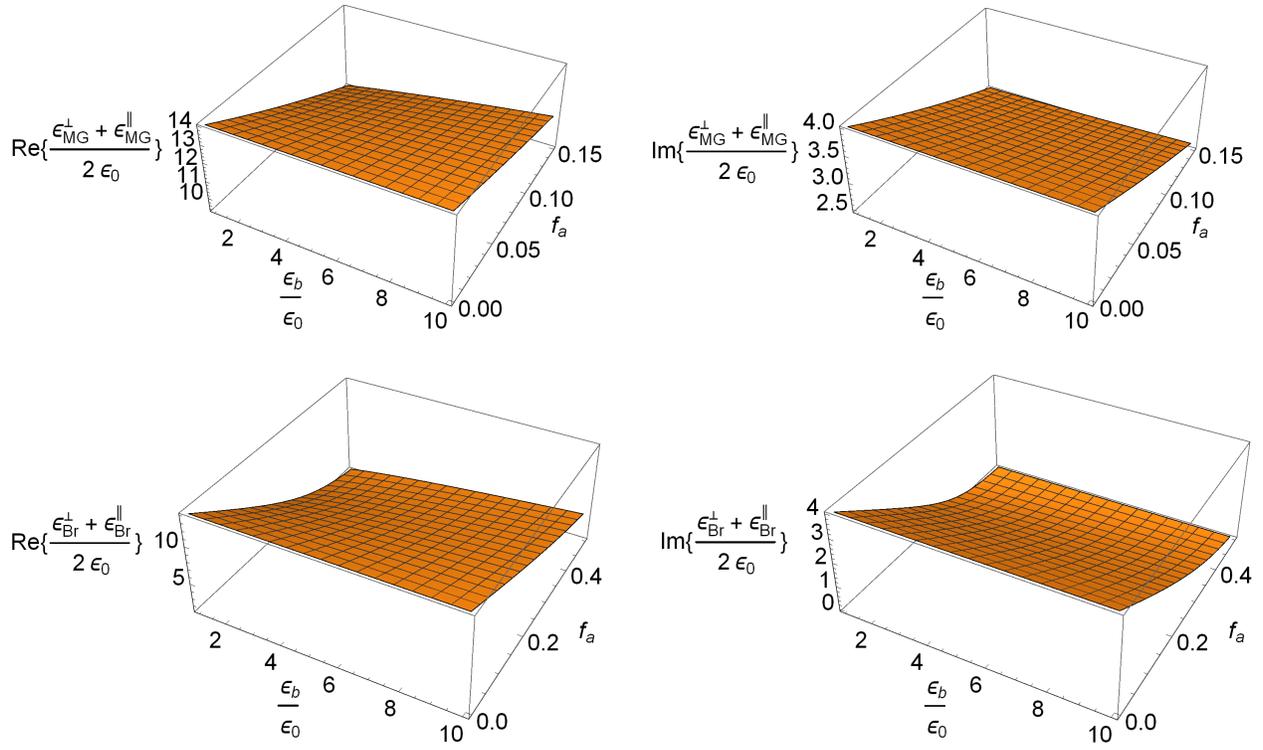


Figure 3: As Fig. 1 except that the dimers are identically oriented and the real and imaginary parts of the averages  $\left(\epsilon_{MG}^\parallel + \epsilon_{MG}^\perp\right)/2\epsilon_0$  and  $\left(\epsilon_{Br}^\parallel + \epsilon_{Br}^\perp\right)/2\epsilon_0$  are plotted.

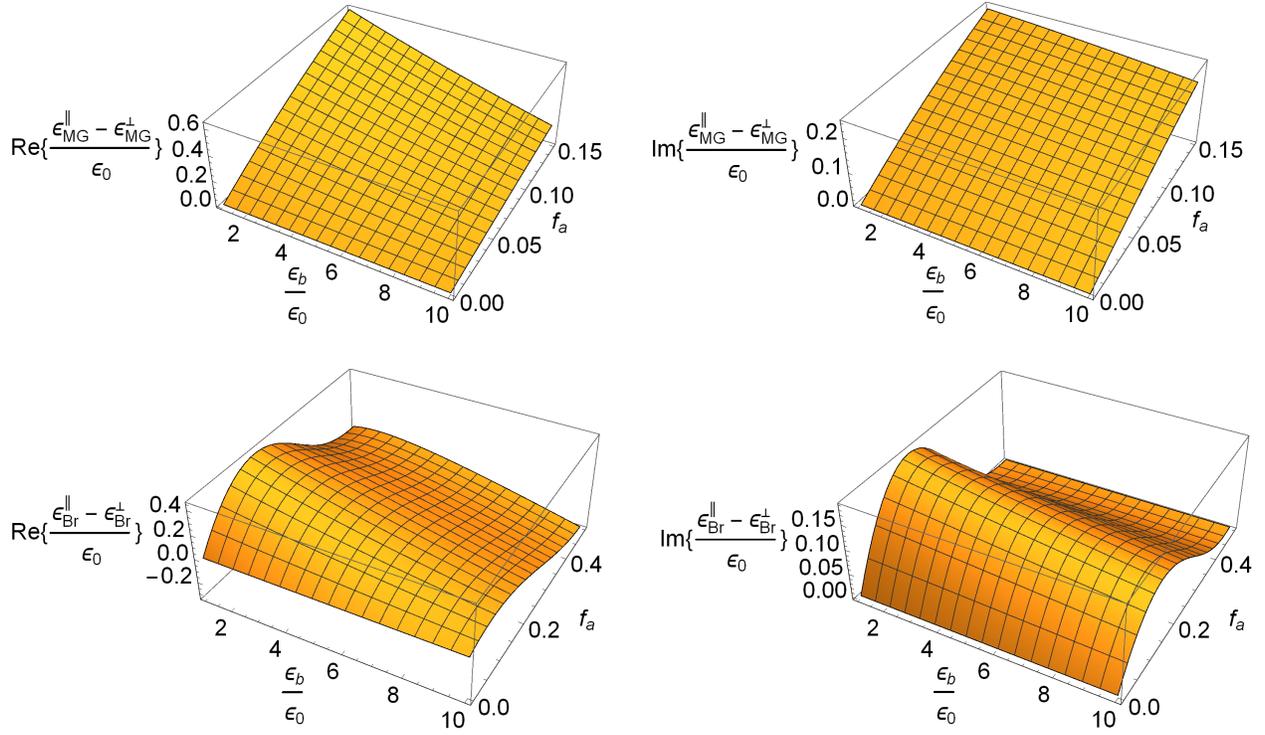


Figure 4: As Fig. 1 except that the dimers are identically oriented and the real and imaginary parts of the differences  $(\epsilon_{MG}^{\parallel} - \epsilon_{MG}^{\perp})/\epsilon_0$  and  $(\epsilon_{Br}^{\parallel} - \epsilon_{Br}^{\perp})/\epsilon_0$  are plotted.

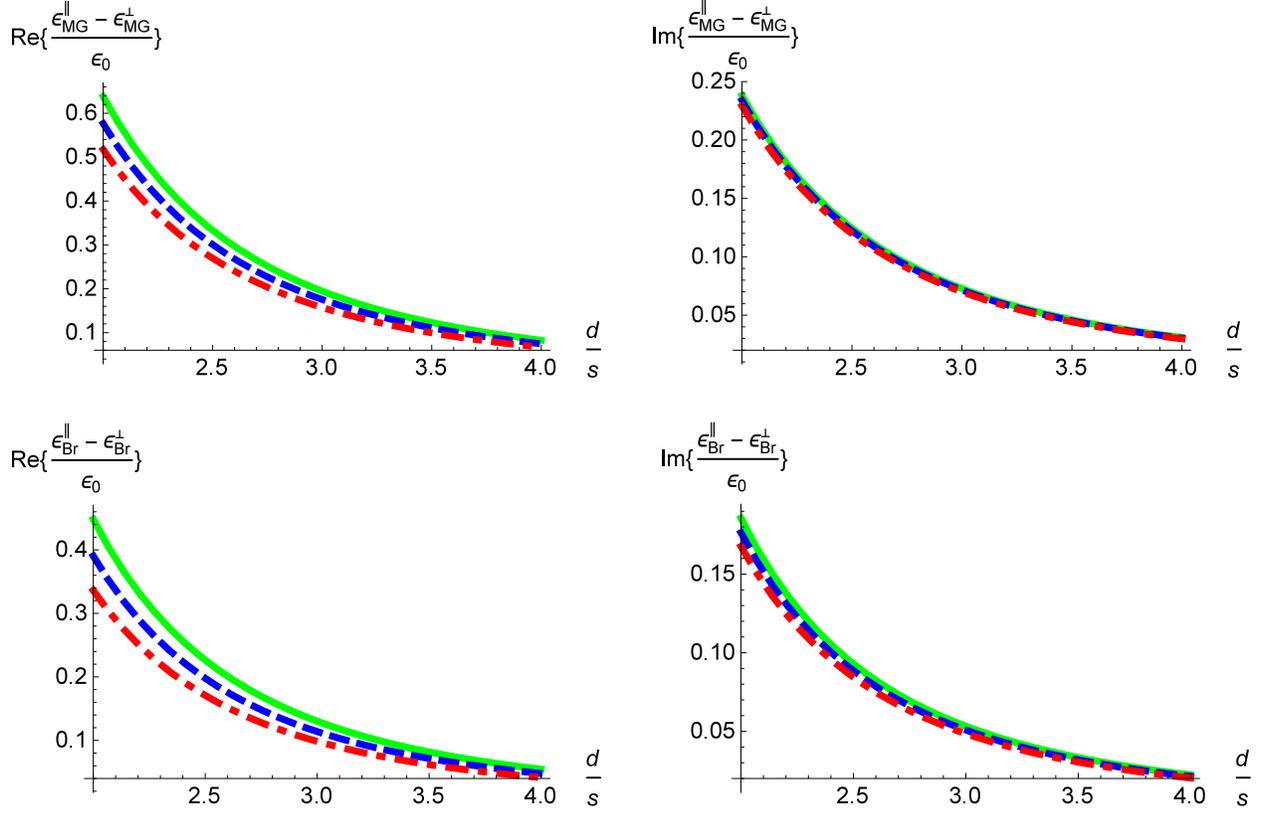


Figure 5: As Fig. 2 except that the dimers are identically oriented the real and imaginary parts of the differences  $(\epsilon_{MG}^{\parallel} - \epsilon_{MG}^{\perp})/\epsilon_0$  and  $(\epsilon_{Br}^{\parallel} - \epsilon_{Br}^{\perp})/\epsilon_0$  are plotted.

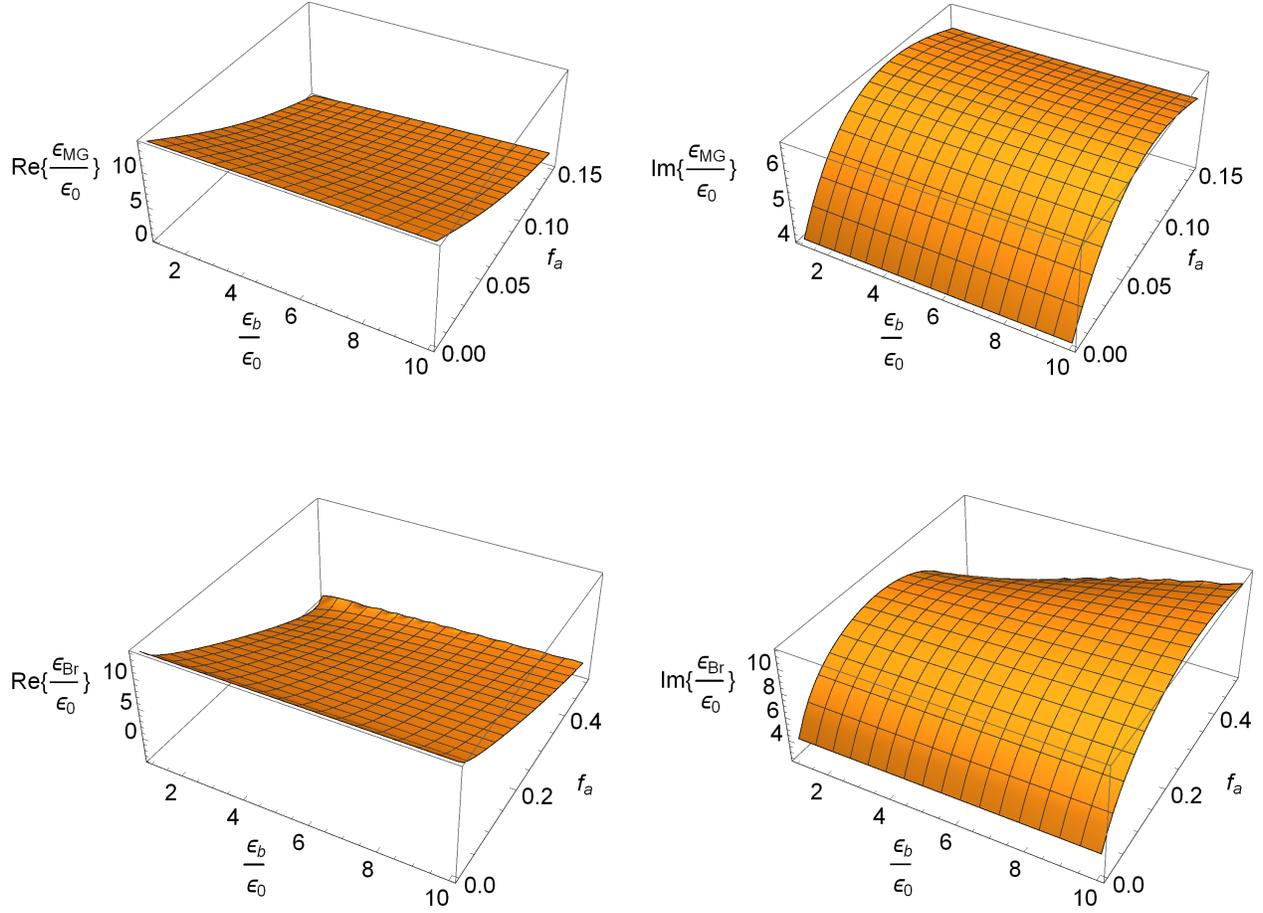


Figure 6: The real and imaginary parts of  $\varepsilon_{MG}/\varepsilon_0$  and  $\varepsilon_{Br}/\varepsilon_0$  plotted against  $\varepsilon_b/\varepsilon_0$  and  $f_a$  for the case where the electrically small spheres of component materials ‘a’ and ‘b’ combine to form metal–dielectric dimers with  $\varepsilon_a = (-21.4 + 2.4i)\varepsilon_0$  (i.e.,  $\varepsilon_a = \varepsilon_{Ag}(5\text{ nm})$  for  $\lambda_0 = 650\text{ nm}$ ) and  $\varepsilon_b \in (1, 10)\varepsilon_0$ . Component material ‘c’ is specified by  $(\varepsilon_c/\varepsilon_0) = 14 + 4i$ . The dimers are randomly oriented and  $d = 2s$ .

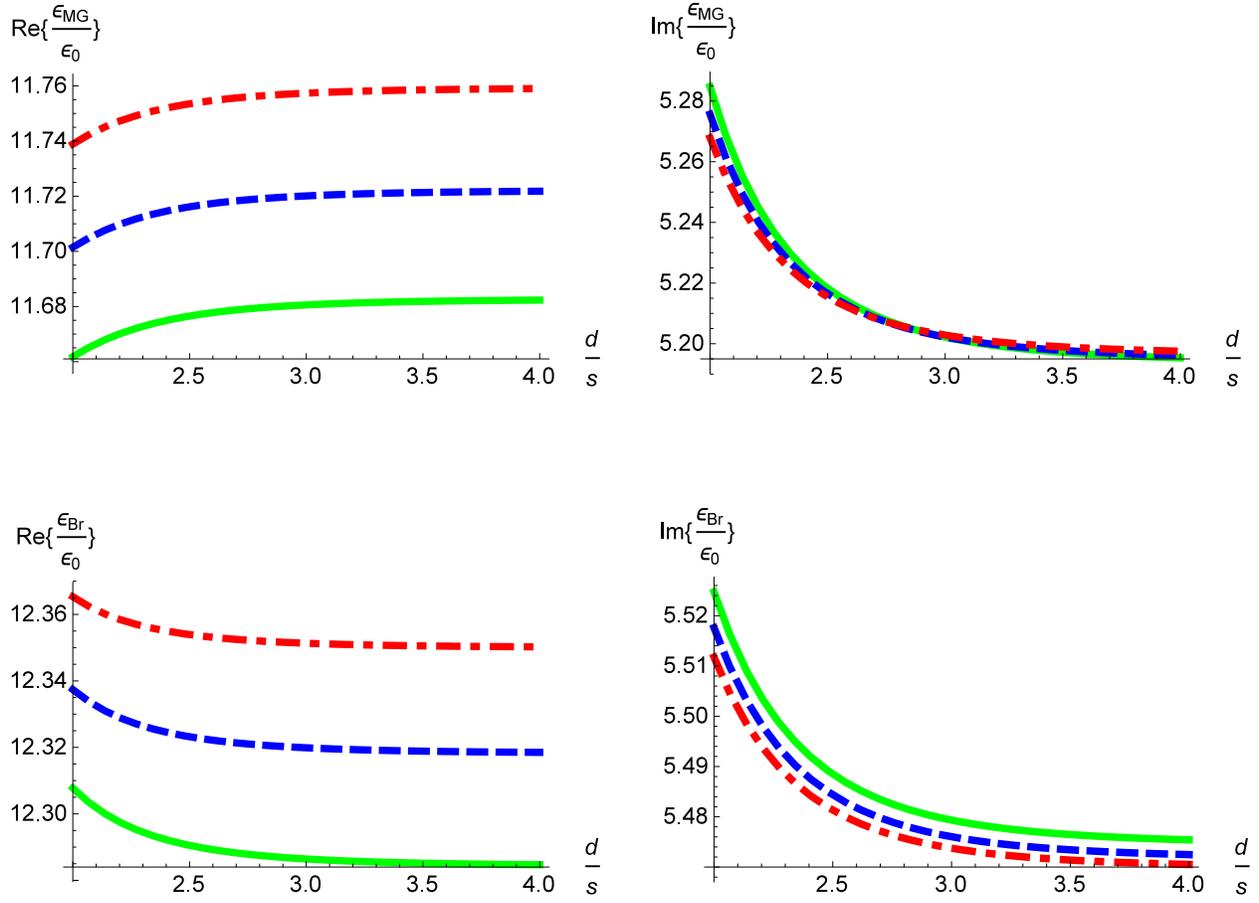


Figure 7: As Fig. 6 except that the real and imaginary parts of  $\epsilon_{MG}/\epsilon_0$  and  $\epsilon_{Br}/\epsilon_0$  plotted against  $d/s$  for  $\epsilon_b = \epsilon_0$  (green, solid curves),  $2\epsilon_0$  (blue, dashed curves), and  $3\epsilon_0$  (red, broken dashed curves). Here  $f_a = 0.02$ .

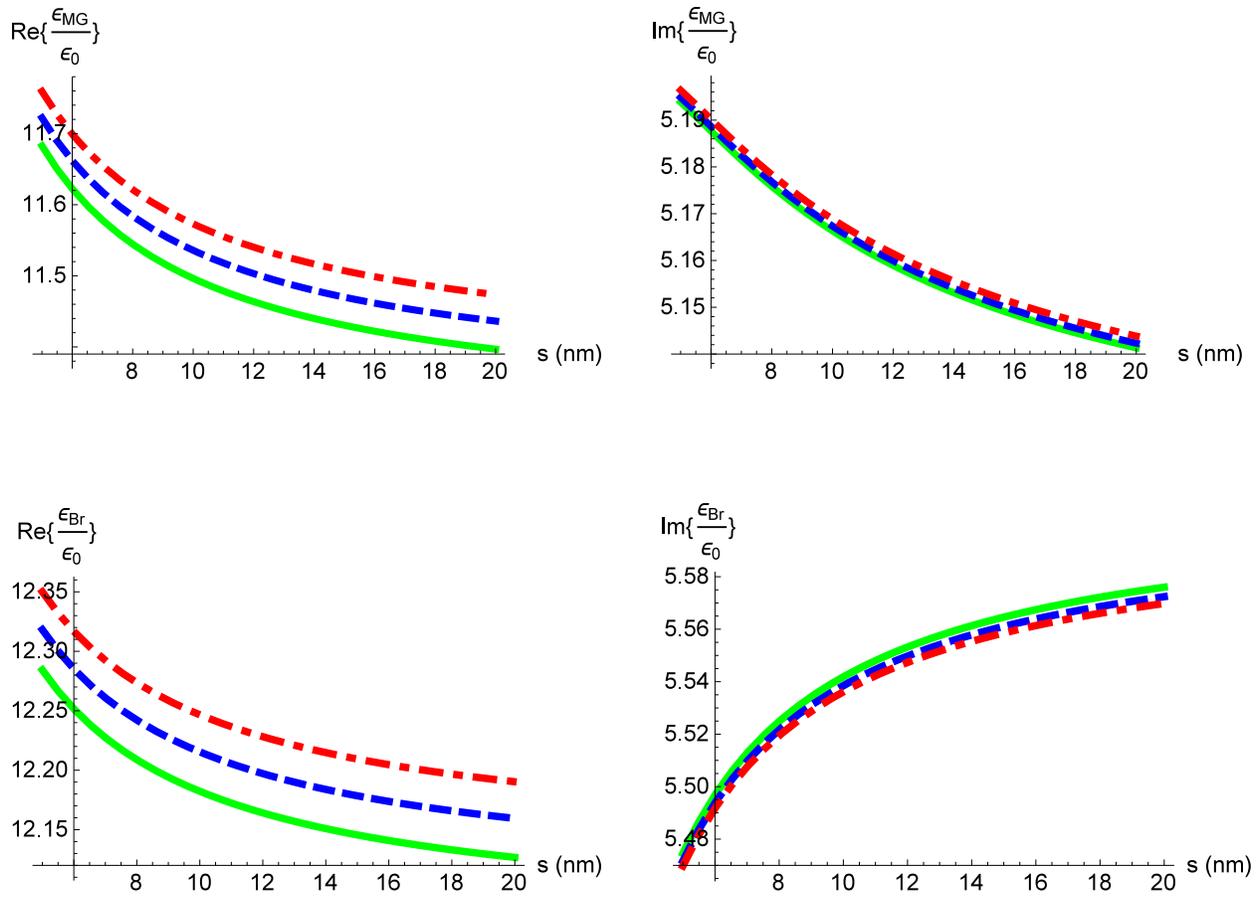


Figure 8: As Fig. 7 except that the real and imaginary parts of  $\epsilon_{MG}/\epsilon_0$  and  $\epsilon_{Br}/\epsilon_0$  are plotted against  $s$  (nm) with  $d = 2s$ .

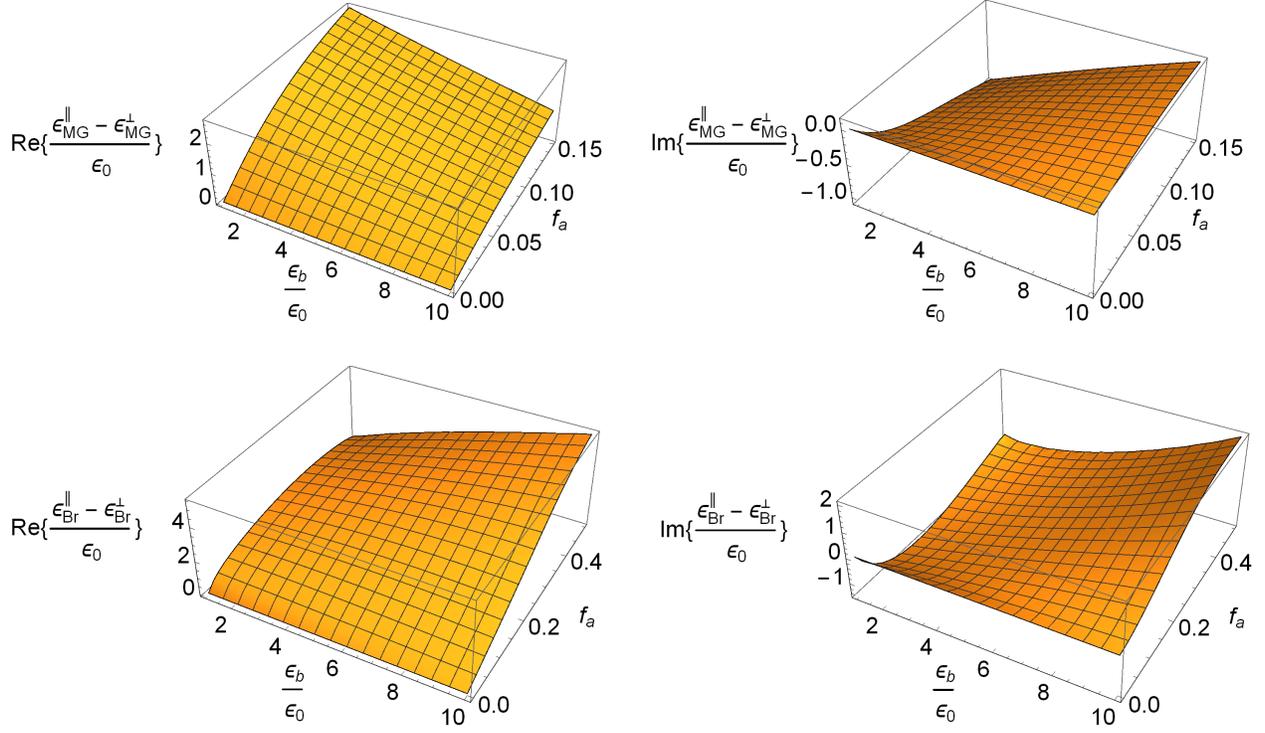


Figure 9: As Fig. 6 except that the dimers are identically oriented and the real and imaginary parts of the differences  $(\epsilon_{MG}^{\parallel} - \epsilon_{MG}^{\perp})/\epsilon_0$  and  $(\epsilon_{Br}^{\parallel} - \epsilon_{Br}^{\perp})/\epsilon_0$  are plotted.

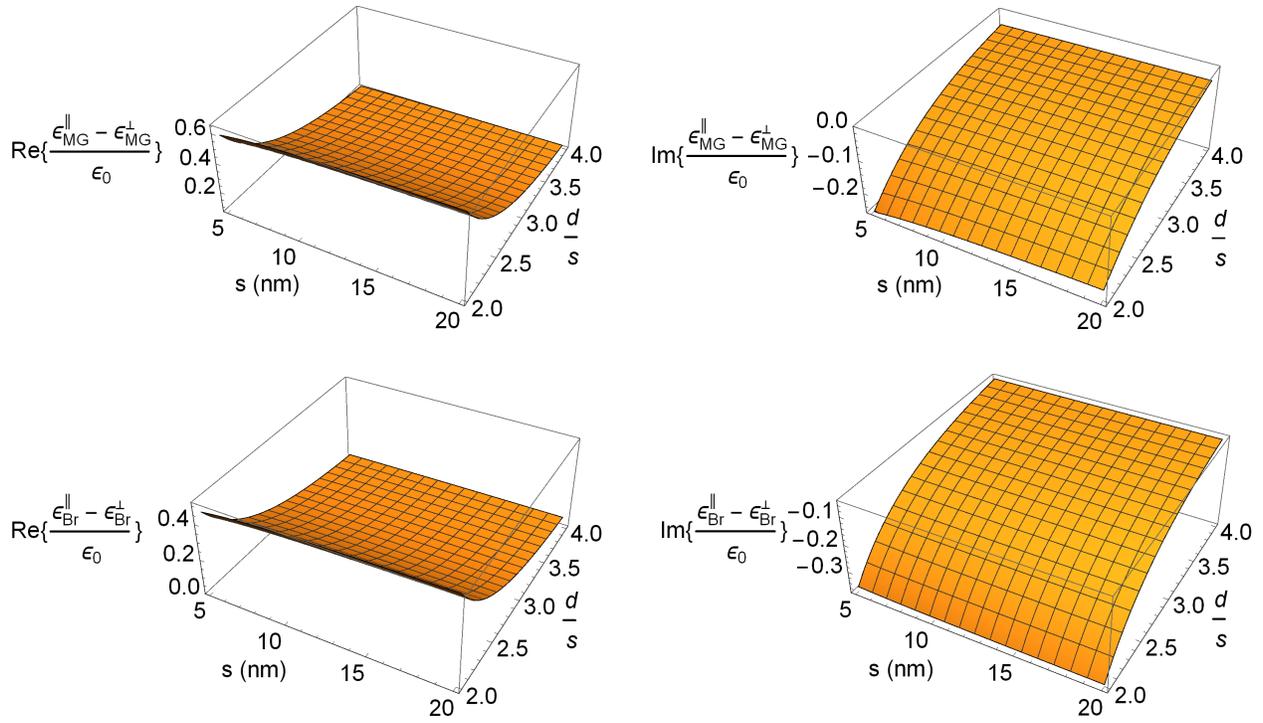


Figure 10: As Fig. 9 except that  $(\epsilon_{MG}^{\parallel} - \epsilon_{MG}^{\perp})/\epsilon_0$  and  $(\epsilon_{Br}^{\parallel} - \epsilon_{Br}^{\perp})/\epsilon_0$  are plotted against  $s$  (nm) and  $d/s$ . Here  $\epsilon_b = 2\epsilon_0$  and  $f_a = 0.02$ .